DOKUZ EYLÜL UNIVERSITY
GRADUATE SCHOOL OF NATURAL AND APPLIED SCIENCES

PERFORMANCE, ECONOMIC AND ENVIRONMENTAL ANALYSES OF INTEGRATED BIOMASS GASIFICATION AND SOLID OXIDE FUEL CELL SYSTEMS

by
Beyza Dursun

December, 2022
İZMİR

PERFORMANCE, ECONOMIC AND ENVIRONMENTAL ANALYSES OF INTEGRATED BIOMASS GASIFICATION AND SOLID OXIDE FUEL CELL SYSTEMS

A Thesis Submitted to the
Graduate School of Natural and Applied Sciences of Dokuz Eylül University
In Partial Fulfillment of the Requirements for the Degree of Master of Science
in Mechanical Engineering, Thermodynamics Program

by

Beyza Dursun

December,2022

İZMİR

M.Sc THESIS EXAMINATION RESULT FORM

We have read the thesis entitled **"PERFORMANCE, ECONOMIC AND ENVIRONMENTAL ANALYSES OF INTEGRATED BIOMASS GASIFICATION AND SOLID OXIDE FUEL CELL SYSTEMS"** completed by **BEYZA DURSUN** under supervision of **PROF.DR. CAN ÖZGÜR ÇOLPAN and PROF.DR.AZİZE AYOL** and we certify that in our opinion it is fully adequate, in scope and in quality, as a thesis for the degree of Master of Science.

Prof. Dr. Can Özgür Çolpan	Prof. Dr. Azize Ayol
Supervisor	Co-Supervisor
Mustafa Asker	Hüseyin Günerhan
Jury Member	Jury Member

Mehmet Akif Ezan

Jury Member

Prof. Dr. Okan FISTIKOGLU

Director

Graduate School of Natural and Applied Sciences

ACKNOWLEDGEMENT

The author wishes to express deep gratitude to co-supervisors Prof. Dr. Can Özgür ÇOLPAN and Prof. Dr. Azize AYOL for their invaluable supervision, advice, encouragement, support, and insight throughout the research process.

The author wishes to express her special thanks to his dear friends Anıl ERDOĞAN, Mert GÜR and Okan GÖK for their valuable contributions to this study.

The author also thanks her dear friend Yağmur Nalbant ATAK for her moral support throughout her postgraduate education and her dear friends Sera Ayten ÇETİNKAYA and Eda KUMCUOĞLU for always being there for her support and assistance.

This thesis was supported by the Scientific and Technological Research Council of Turkey (TUBITAK) 1001 (Grant number: 119R029) Project.

The author gratefully thanks her family for their invaluable support in her entire life.

Beyza DURSUN

PERFORMANCE, ECONOMIC AND ENVIRONMENTAL ANALYSES OF INTEGRATED BIOMASS GASIFICATION AND SOLID OXIDE FUEL CELL SYSTEMS

ABSTRACT

In this study, an integrated system with a SOFC and a gasifier is investigated at the system level. Initially, a zero-dimensional downdraft gasifier model was built through the ASPEN Plus program. This model calculates the molar gas composition and flow rate of syngas generated during the gasification process. Depending on the outputs of this model, the effect of the gasifier temperature on the syngas content was parametrically investigated. Secondly, zero-dimensional models for SOFC and other components are developed in the MATLAB environment. The syngas results obtained in ASPEN Plus were transferred to the system-level code created in MATLAB to simulate the performance of the system. Then, a parametric analysis was performed to examine the effect of gasifier temperature on the performance of the integrated system. Energy and exergy efficiencies were used as the performance parameters. For the baseline circumstances, exergy destruction rate of the system components was also examined. Thirdly, exergo-economic analysis of the integrated system with downdraft gasifier and SOFC was carried out. The effects of parameters such as gasifier temperature, SOFC stack number on the cost of produced electricity were investigated. Finally, greenhouse gas emissions were evaluated from an environmental perspective of the integrated system.

Keywords: Solid oxide fuel cells, gasification, downdraft gasifier, updraft gasifier, performance analysis, exergo-economical analysis, environmental analysis

BÜTÜNLEŞİK BİYOKÜTLE GAZLAŞTIRMA VE KATI OKSİT YAKIT PİLİ SİSTEMLERİNİN PERFORMANS, EKONOMİK VE ÇEVRESEL ANALİZLERİ

ÖZ

Bu çalışmada katı oksit yakıt pili (KOYP) ve gazlaştırıcı içeren entegre bir sistem, sistem seviyesinde incelenmiştir. Başlangıçta, sıfır boyutlu aşağı akışlı gazlaştırıcı ASPEN Plus programı aracılığıyla inşa edildi. Bu model, gazlaştırma işlemi sonucunda üretilen sentez gazının molar gaz bileşimini ve akış hızını verir. Bu program çıktılarına bağlı olarak, gazlaştırıcı sıcaklığındaki değişimin sentez gazı içeriği üzerine olan değişimi parametrik olarak incelenmiştir. İkinci olarak, KOYP ve diğer bileşenler için modeller MATLAB ortamında sıfır boyutlu olarak geliştirilmiştir. ASPEN Plus'ta elde edilen sentez gazı sonuçları, sistemin performansını simüle etmek için MATLAB'da oluşturulan sistem düzeyindeki koda aktarılmıştır. Ardından, gazlaştırıcı sıcaklığının entegre sistemin performansı üzerindeki etkisini incelemek için bir parametrik analiz gerçekleştirilmiştir. Performans parametreleri ekserji verimi, yakıt kullanım verimi ve elektrisel verim olarak belirlenmiştir. Sistem bileşenlerinin ekserji yıkımları da temel koşullar içinde değerlendirilmiştir. Üçüncü olarak aşağı akışlı gazlaştırıcı ve KOYP içeren entegre sistemin eksergo-ekonomik analizi geliştirilmiştir. Gazlaştırıcı sıcaklığı, KOYP yığın sayısı gibi parametrelerin maliyet üzerine etkisi incelenmiştir. Son olarak entegre sistemin çevresel bakış açısı olarak sera gazı emisyonları değerlendirilmiştir.

Anahtar Kelimeler: Katı oksit yakıt pili, gazlaştırma, aşağı akışlı gazlaştırıcı, yukarı çekişli gazlaştırıcı, performans analizi, eksergo-ekonomik analiz, çevresel analiz

CONTENTS

Page

LIST OF FIGURES

Page

LIST OF TABLES

Page

LIST OF SYMBOLS

A	Active surface area [cm^2]
C	Number of components; weight percentage of carbon in biomass
e	Specific exergy [kJ/kg]
ex	Specific molar exergy [J/mole]
$\dot{E}x$	Exergy flow rate [W]
F	Faraday constant [-]
g	Standard gravity [cm/s^2]
$\bar{g}$	Specific molar Gibbs free energy [J/mole]
$\bar{h}$	Specific molar enthalpy [J/mole]
H	Weight percentage of hydrogen in biomass
$\dot{H}$	Enthalpy flow rate [W]
i	Current density [A/cm^2]
i_o	Exchange current density [A/cm^2]
I	Current [A]
k	Thermal conductivity [W/cm-K]
K	Equilibrium constant [-]
L	Thickness of a cell component [μm]
$\dot{m}$	Mass flow rate [g/s]
M	Molecular weight [g/mole]
$\dot{n}$	Molar flow rate [mole/s]
N	Weight percentage of nitrogen in biomass [-]
O	Weight percentage of oxygen in biomass [-]
P	Pressure [kPa]
q	Specific molar heat [J/mole]
$\dot{Q}$	Heat transfer rate [W]
r	Recirculation ratio
R	Universal gas constant [J/mole-K]
s	Specific entropy rate [J/mole-K]
$\dot{S}$	Entropy rate [W/K]

T	Temperature [℃]
U_f	Fuel utilization ratio
U_a	Air utilization ratio
V	Voltage [V]
$\dot{W}$	Power output [W]
x	Molar ratio

Greek Letters

η_{el}	Electrical efficiency
λ	Molar ratio of steam entering the gasifier to the dry biomass
ε	Exergetic efficiency

Subscripts

a	Anode; air
ac	Air channel
act	Activation
b	Boudard
c	Cathode
conc	Concentration
CV	Control volume
D	Destruction
e	Electrolyte; Exit
el	Electrochemical; Electrical
eq	Equilibrium
fc	Fuel channel
F	F
FC	Fuel cell
fi	Fuel channel inlet
g	Gas

gen	Generated
i	Inlet
L	Loss
ohm	Ohmic
mix	Mixture
N	Nernst
o	Standard
P	Product
prod	Product
r	Reaction

ABBREVIATIONS

AFC	Alkaline fuel cell
CHP	Combined heat power
DMFC	Direct methanol fuel cell
DNA	Dynamic network analysis
FUE	Fuel utilization efficiency
FX	Fixed carbon
GHG	Greenhouse gas
HRSG	Heat recovery steam generator
LUCE	Levelized unit cost of electricity
MC	Grid convergence index
MC	Moisture content
MCFC	Molten carbonate fuel cell
MGT	Micro gas turbine
NETL	National energy technology laboratory
ORC	Organic Rankine cycle
OVT	Organic vapor turbine
PAFC	Phosphoric acid fuel cell
PEMFC	Proton exchange membrane fuel cell
SOFC	Solid oxide fuel cell

SPECO	Specific exergy costing
VM	Volatile matter
KOYP	Katı oksit yakıt pili
LHV	Lower heating value
$PR-BM$	Peng Robinson-Boston Mathias

CHAPTER ONE
INTRODUCTION

1.1 Introduction

Today, increasing population and developing technology have rised the global energy demand and consumption, and thus air pollution and climate change issues have become critical. As a result, it has become mandatory to switch to clean renewable and alternative energy resources and their technologies. Solar, wind, geothermal, and biomass energy are a few examples of renewable energy resources. As a carbon-neutral energy resource, biomass has a smaller environmental effect than fossil fuels, which are widely available worldwide (Energy Information Administration, 2019; Tezer et al., 2022).

Biomass consists of carbon-based materials and mixtures of organic compounds. Examples of biomass are agricultural waste, animal waste, food waste, rice husk, municipal solid waste, and wastewater (Begum et al., 2013). One of the methods of converting biomass to useful energy is gasification. In this method, biomass enters the gasifier with air, oxygen or steam and is converted into syngas as a result of a thermochemical process. The most commonly used fixed bed gasifiers are updraft and downdraft gasifiers. In the downdraft gasifier, the biomass is fed from above and the syngas formed leaves from the bottom as both the biomass and air move downstream. In the updraft gasifier, the biomass is still fed from above, but biomass moves downwards, the supplied air moves upwards, and the syngas formed leaves the gasifier from the top. The gasification process is divided into four stages. In the drying process of a typical downdraft gasifier (>150°C), the moisture content of the fuel is reduced by the evaporation process. In pyrolysis (between 200°C and 500°C), products such as coal, H_2, CO, and CH_4 are formed with the heat it receives. During the combustion or oxidation (between 700°C and 1500°C) of coal and other combustible materials, burned gases are released and these high-temperature gases

provide the necessary heat for the other stages. In the reduction stage (between 650°C and 900°C), the gasification reactions that form the syngas occur (Basu, 2010).

Solid oxide fuel cell (SOFC) is a highly efficient electrochemical system operating at high temperature (500-1000°C). SOFC consists of two electrodes separated by an electrolyte made of ceramic material. Oxygen fed from the cathode is reduced to the oxygen ions. These ions move between the electrodes through the electrolyte. At the anode side, hydrogen combines with oxygen ions from the cathode to form water vapor and electrons (Ormerod, 2003). Electricity is produced from the SOFC through the movement of electrons through load.

Recently, interest in integrated systems including solid oxide fuel cell and gasifier has increased and many articles have been published on these systems. In this thesis, a system including solid oxide fuel cell and gasifier was studied. First, the downdraft gasifier model was simulated through the ASPEN Plus program. The obtained syngas results were transferred to MATLAB for the analysis of the SOFC and whole system through zero-dimensional modeling approach. Finally, performance, economic and environmental analyses were conducted for the integrated system.

1.2 Motivation

This thesis focuses on the simulation and modeling of an integrated system that consists of a solid oxide fuel cell and a downdraft gasifier. The main motivation of this thesis is as follows.

In the literature, there are performance, economic and environmental analyzes of integrated systems containing a biomass gasifier and a solid oxide fuel cell. However, in this study, an innovative approach was created for the integrated system model and performance, economic, and environmental analyses were carried out with the integration of different programs. In the literature research, the system model set up in this study was not encountered. In addition, the number of studies on

the investigation of the effect of gasifier temperature, biomass price, and SOFC stack number parameters on the cost of produced electricity through the thermoeconomic analysis approach is quite limited. In this thesis, a thermoeconomic analysis was conducted using the results of the performance analysis. Finally, the GHG emission results of the integrated system were also examined from an environmental point of view.

1.3 Objective

The main purpose of this thesis is to make performance, economic and environmental evaluations of an integrated energy system containing a solid oxide fuel cell and a biomass-fed downdraft gasifier. The main objectives of the thesis are listed below:

- To evaluate the performance of the integrated system through exergy analysis
- To assess the effect of parameters (e.g., SOFC stack number, gasifier temperature, and cell voltage) on the system performance
- To make an economic evaluation of the integrated system having a downdraft gasifier and a SOFC by examining the parameters such as biomass price and SOFC stack.
- To examine the environmental analysis of the integrated system having a downdraft gasifier and a SOFC

1.4 Thesis Outline

In the second chapter, fuel cell technology and gasification process are explained. In this section, the types of fuel cells, types of gasifiers and the gasification process are mentioned in detail, and a literature review including the performance, economic and environmental analyzes of integrated systems containing these components is presented. In the third chapter, the mathematical model of the integrated system including the downdraft gasifier and SOFC is explained. First, the development of a downdraft gasifier model is explained. Secondly, a system-level model including all

components is done. Finally, thermoeconomic and environmental analyses of the integrated system are explained. In the fourth chapter, the results of the performance, economic and environmental analyses of the system containing SOFC and downdraft gasifier are given and discussed. The fifth chapter gives conclusions related to the studies in this thesis.

CHAPTER TWO
BACKGROUND AND LITERATURE SURVEY

2.1 Biomass Energy

Biomass is a type of sustainable biological material derived from plants and animals. Biomass is a significant fuel in many nations, particularly in developing countries for cooking and heating. Many industrialized nations are boosting their use of biomass fuels for transportation and power generation in order to reduce carbon dioxide emissions from fossil fuel consumption. Now biomass energy supplies 10% to 14% of worldwide primary energy, including around 3% of world transportation, but has the possibility of contributing up to 30-40% by 2050, based on the source (Energy Information Administration, 2022).

2.1.1 Biomass Types

As shown in Table 2.1, there are different biomass types. These types broadly encompass all plants and plant-derived compounds, including livestock manure. Primary biomass, also known as virgin biomass, is derived directly from plants or animals. Waste or derived biomass is derived from various biomass-derived products (e.g woody biomass, herbaceous biomass, energy crops, agricultural waste, municipal waste, industrial waste and forestry waste) (Basu, 2010).

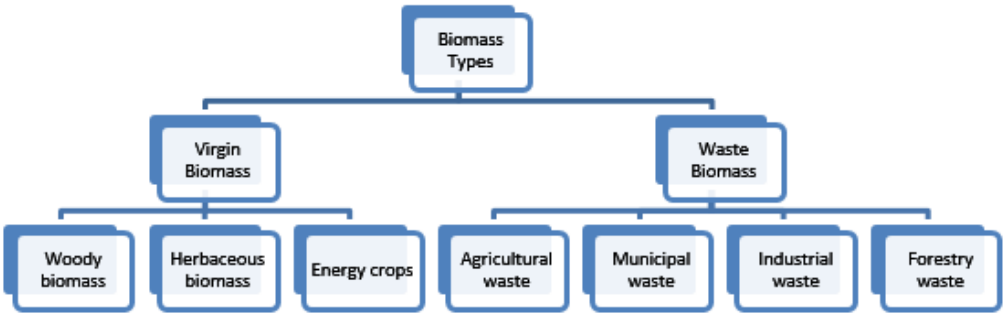

Figure 2.1 Biomass Types (Basu, 2010)

2.1.2 Composition of Biomass

Biomass consists of various compounds such as moisture (M), ash (ASH), nitrogen (N), carbon (C), oxygen (O), hydrogen (H), and small amounts of other compounds (Basu, 2010). Biomass composition is an important parameter when developing a gasifier. The two most common composition analysis methods are ultimate analysis and proximal analysis. The essential constituents of the hydrocarbon fuel are evaluated for the ultimate analysis. Eq (2.1) represents the mass percent of the respective components in the fuel.

$$C + H + O + N + S + Cl + M + ASH = 100\% \quad (2.1)$$

For proximate analysis, the fuel's composition is delivered as volatile matter (VM), moisture (M), fixed carbon (FC), and ash (ASH). The condensable and noncondensable vapor created when the fuel is heated is known as volatile matter. Fixed carbon can be defined as the solid carbon which remains after the pyrolysis process.

$$FC + VM + ASH + M = 100\% \quad (2.2)$$

Ultimate and proximate analysis results calculated for some biomass samples in the literature are shown in Table 2.1.

Table 2.1 Proximate and Ultimate Analyses Results for Different Biomass Types (Erdogan et al., 2022)

		Proximate Analysis (%)				**Ultimate Analysis (%)**				
Author(s)	**Biomass Type**	**Moisture Content**	**Fixed Carbon**	**Volatile Matter**	**Ash**	**C**	**H**	**O**	**N**	**S**
Wilson et al., (2011)	Coffee bean husks	10.1	83.2	14.3	2.5	49.4	6.1	41.2	0.7	0.07
Ramzan et al., (2011)	MSWs	12	15.47	38.29	46.24	36.4	4.97	10.15	1.44	0.802
Gu et al., (2019)	Rice straw	9.3	11.15	83.17	05.68	47.53	05.74	40.14	0.18	0.73
Han et al., (2017)	Hardwood chips	25	19.031	79.850	1.119	49.817	5.556	43.425	0.078	0.005
Begum et al., (2013)	MSWs	12	15.47	38.29	46.24	36.4	4.97	10.15	1.44	0.802

2.2 Energy Production Routes from Biomass

A variety of techniques may be used to convert biomass into usable types of energy. The kind and quantity of biomass feedstock; the required form of energy, i.e. end-use needs; environmental regulations; economic conditions; and project-specific considerations all impact the choice of conversion method. In many cases, the process path is determined by the form in which the energy is required, followed by the available types and amounts of biomass.

As shown in Figure 2.2, the conversion of biomass to energy is accomplished via the use of two primary process technologies: thermo-chemical and bio-chemical/biological. There are four process choices for thermo-chemical conversion: combustion, pyrolysis, gasification, and liquefaction. Bio-chemical conversion includes two processes: digestion (the creation of biogas, which is mostly methane and carbon dioxide) and fermentation (the production of ethanol) (McKendry, 2002).

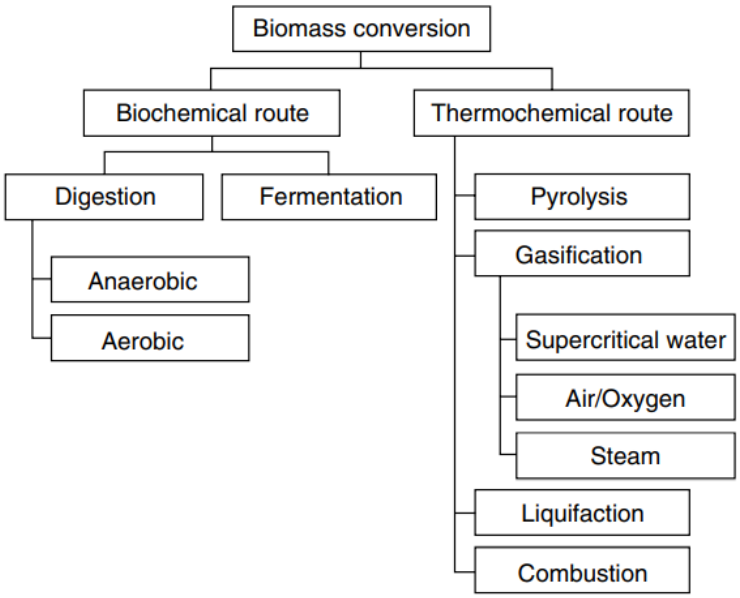

Figure 2.2 Biomass conversion methods (Basu, 2010)

2.3 Gasification

Gasification is the process of obtaining combustible gaseous fuel by the high-temperature decomposition of solid fuels such as carbon-containing biomass. Gasification consists of 4 steps: drying, pyrolysis, partial combustion, and gasification of decomposed products. These steps are summarized in Figure 2.2. The drying process reduces the moisture content of the fuel. In pyrolysis, with the absence of oxygen, products such as coal, H_2, CO, and CH_4 are formed with the heat it receives. During the combustion or oxidation of coal and other combustible materials, burned gases are released and these high-temperature gases provide the necessary heat for the other stages. In the reduction stage, the gasification reactions that produce the syngas occurs. The main reactions which occur in the gasifier are summarized in Table 2.2 (Basu, 2010)

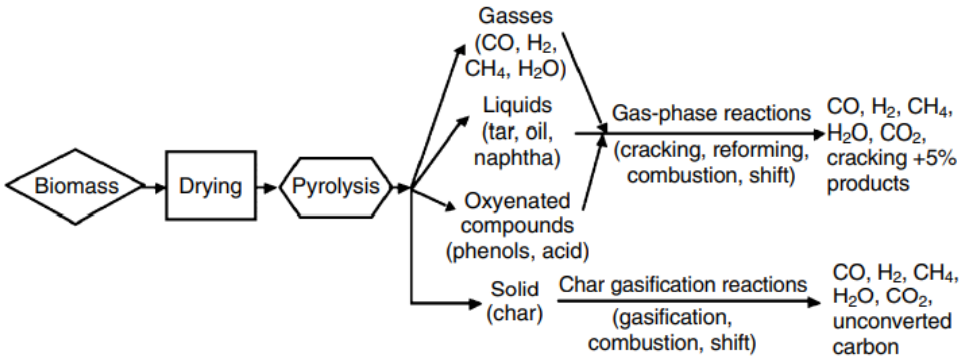

Figure 2.3 Gasification process (Basu, 2010)

Table 2.2 Reactions taking place in the gasifier (Basu, 2010)

Reaction	**Chemical equation**	**Reaction kinetic (mol / m^3)**
Char gasification (R1)	$C + H_2O \leftrightarrow CO + H_2$ (+131 kJ/mol)	$r_f = 1.372 m_s T exp - \left(\frac{22645}{T}\right)[H_2O]$ $r_b = 1.044 \times 10^{-4} m_s T^2 \exp\left(-\frac{6319}{T} - 17.29\right)[H_2][CO]$
Boudouard (R2)	$C + CO_2 \leftrightarrow 2CO$ (+172 kJ/mol)	$r_f = 1.272 m_s T exp\left(-\frac{22645}{T}\right)[CO_2]$ $r_b = 1.044 \times 10^{-4} m_s T^2 exp\left(-\frac{2363}{T} - 20.92\right)[CO_2]$
Methane decomposition (R3)	$\frac{1}{2}CH_4 \leftrightarrow \frac{1}{2}C + +H_2$ (+74.8 kJ/mol)	$r_f = 0.151 m_s T^{0.5} exp\left(-\frac{13578}{T} - 0.372\right)[CH_4]^{0.5}$ $r_b = 1.368 \times 10^{-3} m_s T exp\left(-\frac{8078}{T} - 7.087\right)[H_2]$
Water-gas shift (R4)	$CO + H_2O \leftrightarrow CO_2 + H_2$ (-41.2 kJ/mol)	$r_f = 7.68 \times 10^{10} exp\left(-\frac{36640}{T}\right)[CO]^{0.5}[H_2O]$ $r_b = 6.4 \times 10^9 exp\left(-\frac{13578}{T} - 0.372\right)[H2]^{0.5}[CO_2$
Steam reforming (R5)	$CH_4 + H_2O \leftrightarrow CO + 3H_2$ (+206 kJ/mol)	$r_f = 3.0 \times 10^5 T exp\left(-\frac{15042}{T}\right)[CO]^{0.5}[H_2O]$ $r_b = 0.0265\, T\, exp\left(-\frac{32900}{T}\right)[CO][H_2]^2$

2.3.1 Gasifier Types

Gasifiers are categorized into three types based on their gas-solid contacting mode: (i) fixed or moving bed gasifiers, (ii) fluidized bed gasifiers, and (iii) entrained-flow bed gasifiers (Basu, 2010).

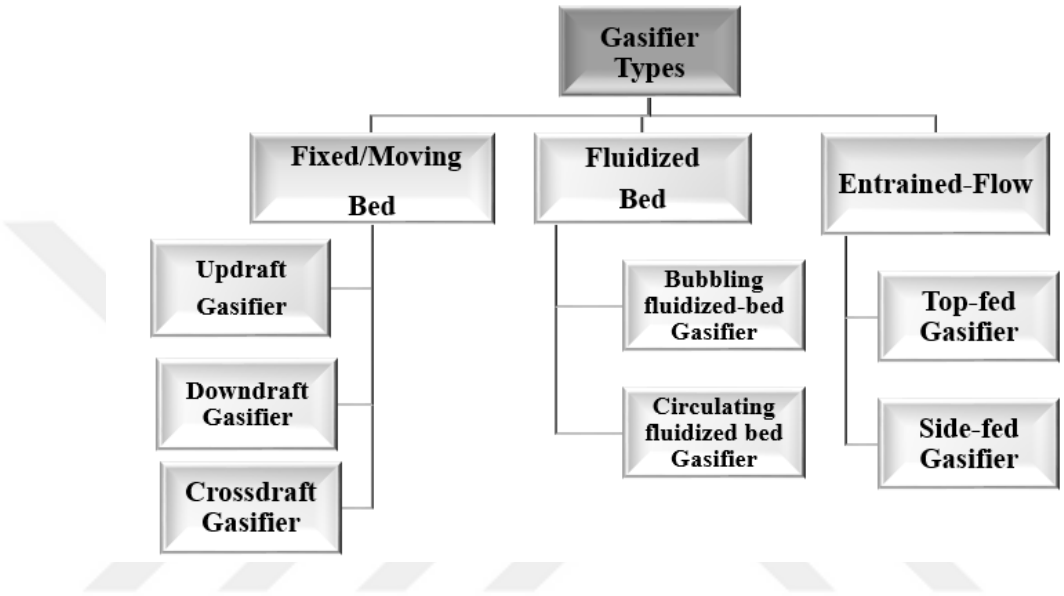

Figure 2.4 Gasifier Types

2.3.1.1 Fixed-Bed/Moving Bed Gasifiers

The most preferred gasifiers for creating synthesis gases are fixed-bed or moving-bed gasifiers. This sort of gasifier is simple to construct and run. Furthermore, fixed-bed gasifiers may be produced in modest sizes. Because of these benefits, they are frequently employed in industry.

2.3.1.1.1 Downdraft Gasifiers

For a downdraft gasifier, biomass is fed from above and syngas formed leaves from the bottom as both biomass and air move downstream. Figure 2.5 (a) shows a schematic of a downdraft gasifier. The gasification process is generally divided into

four stages. In the drying process of a typical downdraft gasifier (>150°C), the moisture content of the fuel is decreased by the evaporation process. In pyrolysis (between 200°C and 500°C), products such as coal, H_2, CO, and CH_4 are formed with the heat it receives. During the combustion or oxidation (between 700°C and 1500°C) of coal and other combustible materials, burned gases are released and these high-temperature gases provide the necessary heat for the other stages. In the reduction part (650°C -900°C), the gasification reactions that form the syngas occurs (Basu, 2010).

2.3.1.1.2 Updraft Gasifier

Figure 2.5 (b) demonstrates the updraft gasifier. The feed is delivered from the top of these gasifiers, and the air is fed from the bottom via the grate. Feed and air move counter currently in the gasifier. The bottom section of the gasifier is effectively the "combustion" zone, where the char created as a result of drying and devolatilization of biomass is burned. This contributes to an increase in the temperature of the bottom area of the gasifier to around 727 °C. In the area immediately above the combustion zone, hot gases moving upward through the bed of downflowing biomass are minimized. The heated gases farther up the gasifier pyrolyze and dry the biomass. These operations reduce the temperature of the gases to around 200-300 °C (Choudhury et al., 2015).

2.3.1.1.3 Crossdraft Gasifier

As seen in Figure 2.5 (c), a cross-draft gasifier is a co-current moving-bed reactor in which fuel is delivered from the top and air is injected from the side via a nozzle. Its primary use is the gasification of charcoal with a low ash level. High-velocity air enters the gasifier by a nozzle located a specified distance above the grate. Excess oxygen in front of the nozzles promotes char combustion (oxidation), resulting in an extremely high-temperature (>1500 °C) zone. In the following zone, the leftover char is gasified to CO. The product gas leaves the gasifier from the other side. The heat

from the combustion zone is directed around the pyrolysis zone, pyrolyzing the biomass as it passes through it (Basu, 2010).

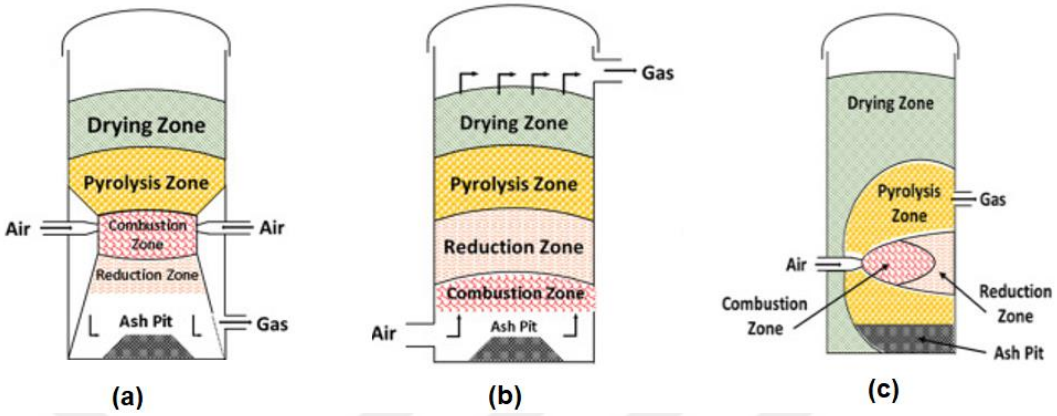

Figure 2.5 Schematic of (a) downdraft gasifier (b) updraft gasifier (c) cross-draft gasifier (Kumari & Karmee, 2022)

2.4 Fuel Cell

Fuel cells are environmentally friendly and efficient devices that directly convert the energy of the fuel into electrical energy by means of an electrochemical reaction (Colpan et al., 2008b). As illustrated in Figure 2.6, a unit cell, consists primarily of three components which are listed as anode, cathode, and electrolyte. The anode and cathode are constantly supplied with fuel and air, respectively. Ions formed during electrochemical processes at one electrode are transmitted to the other electrode via the electrolyte. A load is used to cycle electrons. The movement of electrons produces an electric current, which performs work on the load.

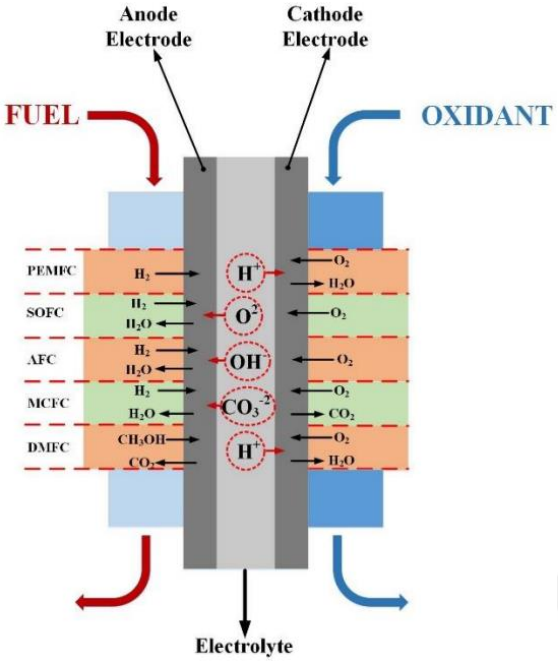

Figure 2.6 Fuel Cell Types (Colpan et al., 2018)

There are different types of fuel cells. They are divided into six primary classes based on the fuel and electrolyte used (Mekhilef et al., 2012) :

- Proton exchange membrane fuel cell (PEMFC)
- Alkaline fuel cell (AFC)
- Direct methanol fuel cell (DMFC)
- Solid oxide fuel cell (SOFC)
- Molten carbonate fuel cell (MCFC)
- Phosphoric acid fuel cell (PAFC)

2.4.1 Proton Exchange Membrane Fuel Cell (PEMFC)

In a typical PEMFC, while hydrogen gas enters the anode, air flows through the cathode and positive ions pass through the electrolyte. While the produced electrons flow through an external circuit, protons flow from one electrode to the other towards the electrolyte. Water is formed by combining protons and electrons with

oxygen flow at the cathode. The reactions taking place in PEMFCs are as summarized in Eqs. (2.3) and (2.4) (Mekhilef et al., 2012).

$$\text{Anode: } H_2 \rightarrow 2H^+ + 2e^- \tag{2.3}$$

$$\text{Cathode: } {}^{1}/_{2}\, O_2 + 2H^+ + 2e^- \rightarrow H_2O \tag{2.4}$$

PEMFCs operate at low temperatures (60-100℃). They are light and compact in addition to their fast commissioning. When the efficiency values are examined, it has been discovered that as the working temperature rises, so does the efficiency. PEMFCs have an efficiency rating between 40% and 50%, and their output power can exceed 250 kW. PEM fuel cells are viable alternatives for automotive, small-scale distributed stationary power production, and portable power applications (Barbir, 2005).

2.4.2 Direct Methanol Fuel Cell (DMFC)

The direct methanol fuel cell (DMFC) operates at low temperatures (30-100 ℃) and has a quick refueling system. The fuel of a DMFC is a diluted methanol solution. This solution is converted to carbon dioxide (CO_2) at the anode, while water or steam is generated at the cathode utilizing oxygen from the air. The main reactions taking place in DMFCs can be seen in Eqs. (2.5) and (2.6) (Mekhilef et al., 2012).

$$\text{Anode: } CH_3OH + H_2O \rightarrow CO_2 + 6H^+ + 6e^- \tag{2.5}$$

$$\text{Cathode: } {}^{3}/_{2}\, O_2 + 6e^- + 6H^+ \rightarrow 3H_2O \tag{2.6}$$

2.4.3 Alkaline Fuel Cell (AFC)

The Alkaline Fuel Cell (AFC) generally produces electricity by using the potassium hydroxide (KOH) in a solution based on water. The KOH electrolyte, which is utilized in AFCs in concentrations ranging from 30 to 45 weight percent, provides an advantage over acidic fuel cells. The oxygen reduction kinetics in alkaline electrolytes are substantially quicker than that in acidic electrolytes, making

AFC a more efficient choice (Carrette et al., 2000). As shown in Eqs. (2.7) and (2.8), oxidation takes place at the anode and reduction at the cathode (Mekhilef et al., 2012).

$$\text{Anode: } 2H_2 + 4OH^- \rightarrow 4H_2O + 4e^- \tag{2.7}$$

$$\text{Cathode: } O_2 + 2H_2O + 4e^- \rightarrow 4OH^- \tag{2.8}$$

AFCs typically run at temperatures ranging between 60-90 °C. As an electrolyte, AFC employs an alkaline-based solution such as NaOH or KOH. AFCs have an electrical efficiency of around 60-70% (Abdelkareem et al., 2021).

AFC was one of the first fuel cells used in space. Later, the Gemini program used a PEM fuel cell, but it was quickly recognized that AFC had many advantages over this technology. The AFC was used in the Apollo missions, the Space Shuttle program, and the European Project Hermes (Carrette et al., 2000).

2.4.4 Solid Oxide Fuel Cell

SOFC is a high-temperature (800°C to 1000°C) fuel cell with a high operational efficiency of 60-65%. In SOFCs, solid-ceramic based material (e.g yttrium-stabilized zirconium) is used as the electrolyte. SOFCs can use many fuels such as hydrogen, natural gas, biogas, and coal gas (Carrette et al., 2000). For a hydrogen fed SOFC, the reactions taking place at the anode and cathode are given in Eqs. (2.9) and (2.10).

$$\text{Anode: } O^{2-} + H_2 \rightarrow H_2O + 2e^- \tag{2.9}$$

$$\text{Cathode: } {}^1\!/_2\, O_2 + 2e^- \rightarrow O^{2-} \tag{2.10}$$

SOFCs have several advantages such as 1) easier to manage because there is no fluid in the liquid phase, (2) cheaper materials and methods for producing electro-catalysts, (3) better thermal integration with other energy systems, (4) operation with various fuels such as hydrocarbons, ammonia, alcohols, and biogas, and (5) reformation of carbon-containing gases inside the fuel cell into hydrogen and carbon

monoxide. In addition to its advantages, the key challenges with this fuel cell design include manufacturing difficulties, carbon deposition, and sulfur poisoning issues. SOFCs are mostly used for stationary power and heat generation. Furthermore, it has the potential to be employed in transportation, military, and portable applications (Erdogan et al., 2022).

2.4.5 Phosphoric Acid Fuel Cell (PAFC)

In phosphoric acid fuel cells (PAFC) mostly liquid phosphoric acid (H_3PO_4) electrolytes are used. Because phosphoric acid has a limited ionic conductivity at low temperatures, PAFC can work in the 150-220°C temperature range. The electrolyte transports hydrogen (H+) from the anode to the cathode, and the electrical current is created when the ejected electrons back to the cathode through the outer circuit. Finally, water forms on the cathode (Mekhilef et al., 2012).

$$\text{Anode: } 2H_{2(g)} \rightarrow 4e^- + 4H^+ \tag{2.11}$$

$$\text{Cathode: } O_2 + 4H^+ + 4e^- \rightarrow 2H_2O \tag{2.12}$$

PAFC systems with capacities of up to 200 kW are already in commercial use, while systems with around 11 MW have previously been analyzed. PAFCs are costly to produce because of the requirement for finely distributed platinum catalyst on the electrodes. In contrast to AFCs, the impurity hydrogen vapor (CO_2) has no impact on PAFCs. These fuel cells have an electrical efficiency of 40 to 50% and a CHP efficiency of approximately 85%. PAFCs mainly utilized for stationary on-site applications.

2.4.6 Molten Carbonate Fuel Cell (MCFC)

Molten carbonate fuel cells (MCFCs) operate at high-temperatures (600-700°C). In an MCFC, the electrolyte is a molten alkali carbonate, such as lithium or potassium carbonate, held in a ceramic matrix of lithium aluminum oxide (Revankar

& Majumdar, 2016). The following summarizes the electrochemical processes of MCFC:

$$\text{Anode: } H_2 + CO_3^{2-} \rightarrow H_2O + CO_2 + 2e^- \quad (2.13)$$

$$\text{Cathode: } {}^1/_2\, O_2 + CO_2 + 2e^- \rightarrow CO_3^{2-} \quad (2.14)$$

By creating hydrogen through a reforming process, MCFCs may operate not only with hydrogen but also with other fuel types such as natural gas, biogas, and clean coal gas. Large stationary power generating and CHP are two applications (Revankar & Majumdar, 2016).

2.5 Fuel Cell Applications

The type of fuel cell used determines the uses of fuel cells. With various fuel cell technologies available, determining which innovation is better suited to a certain implementation is critical. Fuel cells have a power range from W to MW scale, allowing them to be used in practically any energy-demanding applications. They can be found in low-power devices as well as consumer gadgets such as mobile phones and laptop computers (PCs). Fuel cell automobiles, household appliances, military uses, and public transit are examples of medium-scale power applications, while cogenerative systems are examples of high-power applications. Due to their versatility, PEMFCs have the greatest variety of applications. Because of their high power density, quick start-up time, high efficiency, low operating temperature, and easy and safe handling, PEMFCs are the most attractive choices for transportation applications. PEMFCs, on the other hand, are still too expensive to be competitive or economically viable. Although AFCs function best when operated on pure hydrogen and oxygen, their sensitivity to contaminants (particularly carbon oxides) and short lifetimes limit their use in terrestrial applications (they are predominantly used for extraterrestrial purposes). Phosphoric acid fuel cells (PAFCs) are arguably the most commercially produced intermediate-temperature fuel cells. PAFCs are utilized in high-energy-efficiency combined-heat-and-power (CHP) applications. High-temperature fuel cells such as molten carbonate fuel cells (MCFCs) and solid oxide

fuel cells (SOFCs) are suitable for cogeneration and combined cycle systems (Sharaf & Orhan, 2014). Table 2.3 lists the principal uses.

Table 2.3 Fuel Cell Applications (Abdelkareem et al., 2021)

Fuel Cell Type	**Operating Temperature (℃)**	**System Output (kW)**	**Electrical Efficiency (%)**	**Applications**	**Advantages**
Alkaline (AFC)	23-70	10-100	60-70	Military Submarines Spacecraft	High activity Can use a variety of catalysts Fast kinetics
Phosphoric Acid (PAFC)	150-200	50-1000	55	Distributed generation	Higher overall efficiency with CHP Higher tolerance to CO_2 High stability
Solid Oxide (SOFC)	600-1000	5-3000	60-65	Auxiliary power Electric utility Large distributed generation	High efficiency Fuel flexibility Can use a variety of fuel
Molten Carbonate (MCFC)	550-700	<1-1000	45-47	Electric utility Large distributed generation	High efficiency Fuel flexibility Can use a variety of catalysts Suitable for CHP

Table 2.3 continues

Polymer Electrolyte Membrane (PEM)	50-100	1-500	50-70	Backup power Portable power Small distributed generation Transportation	Vast power range Easy scale-up Short start-up time High power density
Direct Methanol (DMFC)	30-100	0.001-1	20-30	Replace batteries inmobiles; other portable devices	No CO_2 emission Low start-up time High energy density

2.6 Literature Survey

Recently, it is a preferred method to feed the rich syngas obtained after the gasification process to the fuel cells and obtain electricity. Compared to other technologies, systems containing SOFC and biomass gasifiers reach higher electrical efficiency values than the systems containing gasifiers and internal combustion engines (Ud Din & Zainal, 2016). These systems also have some advantages. Since the developments in the industry also cause electricity demand, integrated systems which include a SOFC and a gasifier are an important factor in reducing air pollution and the need for fuel. In the literature, there are various studies on integrated energy systems including SOFC and biomass gasifier. Toonssen et al. (2011) examined four different systems including a biomass gasifier and a SOFC. The first technology combined large-scale steam gasification with low-temperature gas purification. A large-scale gasifier using air as the gasification agent was also incorporated in the second system, as was low-temperature gas cleaning. A high-temperature gas cleaning system and an air-used gasifier were also added in the third system. Finally, a small-scale air-use gasifier and high-temperature gas cleaning were integrated in the fourth system. In addition, all systems also had a gas turbine. When performance analysis was performed using exergy analysis for all systems, the system with a large scale gasifier using air as the gasification agent and high temperature gas cleaning reached the highest efficiency value with an electrical exergy efficiency value of 49.9%. Rokni, (2014b) studied an integrated system which consists of a downdraft biomass gasifier, an SOFC and a Stirling engine. According to the thermodynamic data calculated using the Dynamic Network Analysis (DNA) simulation tool, the thermal efficiency was found to be 0.41. Bang-Møller & Rokni (2010) studied three different Combined Heat Power (CHP) systems. Configurations consist of a Biomass Gasifier-Micro Gas Turbine (MGT), Biomass Gasifier- MGT and Biomass Gasifier-SOFC-MGT, respectively. The electrical efficiency of these systems was calculated using the DNA approach. The results were found to be 28.1% for the Gasifier-MGT system, 36.4% for the Gasifier-SOFC system, and 50.3% for the Gasifier-SOFC-MGT system. Wongchanapai et al. (2012) examined a hybrid system which consists of a biomass gasifier, SOFC, burner, Heat Recovery Steam Generator (HRSG) and

compressors. Thermodynamic modeling was used for performance evaluation. The efficiency value of a system was found to be 38.9% under optimum performance. Ebrahimi et al. (2016) worked with a system including a gasifier, an SOFC, a Stirling engine, a gas turbine, an Organic Rankine Cycle (ORC) and a Multi-effect distillation.

The studies on energy and exergy analyses performed for integrated biomass gasifier and SOFC systems and their results are listed in Table 2.4.

Table 2.4 The recent studies for energy and exergy analyses of SOFC-biomass gasifier-based integrated systems (Erdogan et al., 2022)

Author(s)	**Year**	**Biomass Type**	**Main System Components**	**Analysis**		**Results**	
				Energy	**Exergy**	**Energy Eff.**	**Exergy Eff.**
Bang-Møller & Rokni, (2010)	2010	Wood chips	Biomass Gasifier, SOFC, MGT	✓	✓	79.7%	68.7%
Toonssen et al., (2011)	2011	Wood	Biomass Gasifier + SOFC + Gas Turbine	✓	✓	-	49.4%
Pierobon et al., (2013)	2013	Wood chips	Biomass Gasifier, SOFC, ORC	✓	X	56.4%	-
Rokni, (2014a)	2014	Wood chip	Biomass Gasifier, SOFC, Stirling Engine	✓	X	42.4%	-
Siefert & Litster, (2014)	2014	Biogas	Biomass Gasifier, SOFC	✓	✓	-	~60%
Ozcan & Dincer, (2015)	2015	Gaseous fuels	Biomass Gasifier, SOFC, ORC, ARC	✓	✓	78%	50%

Table 2.4 continues

Gholamian et al., (2016)	2016	Municipal solid waste	Biomass Gasifier, SOFC, CCHP system	✓	✓	81%	39.35%
Perna et al., (2018)	2017	Wood chips	Biomass Gasifier, SOFC, Micro Gas Turbine	✓	X	88%	-
Lv et al., (2019)	2018	Wood chip	Biomass Gasifier, SOFC, gas turbine	✓	X	60.78%	-
Ghaffarpour et al., (2018)	2018	Pine saw dust, Municipal solid waste, etc.	Biomass Gasifier, SOFC, ORC, gas turbine, HRSG	✓	✓	22.4%	22.7%
Hosseinpour et al., (2018)	2018	Wood	Biomass Gasifier, SOFC, Goswami Cycle	✓	✓	60.2%	34.7%

Several studies on the economic analysis of integrated SOFC and biomass gasification systems have been performed in the literature. Ozgoli et al. (2017) performed an economic analysis of a biomass gasifier-SOFC-gas turbine hybrid system. The results were obtained by using the cost functions separately for each subsystem. A system including biomass gasification, SOFC, and gas turbine was suitable for use in cities in Europe where the cost of electrical energy is high. The estimated cost of the facility was found as $2.53/W. Abuadala & Dincer (2011) studied exergo-economic analysis of a hybrid SOFC-biomass gasification system. SPECO approach was used, and exergy unit costs were obtained for each component of the system. As a result of the study, it was observed that the unit hydrogen cost decreased from 0.258 to 0.211 $/kWh as the hydrogen yield increased from 13.7 to 16.6 kg/h. Morandin et al. (2013) managed the thermo-economic design optimization of a hybrid gasifier-SOFC system. In this study, different configurations were created with various components (reformer, gas turbine, heat recovery steam cycle). Based on the results obtained, it was determined that the configuration mainly including a fluidized bed gasifier, a steam reformer, a pressurized SOFC, and a gas expander was the most suitable configuration. In this configuration, the efficiency reaches the level of 65% with an investment cost of $450,000 at 60 kW power. Rokni (2014b) examined the thermo-economic analysis of a hybrid system in his study. The system included a SOFC, a Stirling engine, and a gasifier. The operating cost per hour was obtained by using the cost equations for each component. The results were found to be 1.752 $/h for the SOFC, 1.5 $/h for the gasifier, 1.217 $/h for the cathode air preheater, and 0.833 $/h for the Stirling engine. The operating cost of the entire system was found as 9,447 $/h. Karimi et al. (2020) worked on a hybrid gasifier-SOFC system with three different configurations. These configurations include a SOFC, a gasifier, a micro gas turbine, and an organic Rankine cycle. The economic analysis done in these studies includes the initial capital costs and maintenance costs of the equipment. An annual evaluation was made for all costs and revenues. The effect of the fuel utilization factor in the calculated economic analysis results was examined. According to these results, it was observed that the cost ratio increased from 11.7 $/hr to 12.4 $/hr as the fuel utilization factor increased from 0.7 to 0.9. Jia et al. (2018) examined the economic feasibility of an integrated energy system

including a micro gas turbine, a solid oxide fuel cell (SOFC), and a biomass gasifier using the net present value (NPV) method. NPV is defined as the sum of the present values of the net cash flows to and from the system over the life of a system. In the study, a mixture of wood chips and animal manure was used as fuel. As a result of the techno-economic analysis, although the cost of the animal manure used in the mixture fuel is lower than the wood chip, the higher percentage of use did not create a more profitable result. CHP power systems are more competitive as SOFC's initial investment and O&M costs are reduced. The payback period was found to be less than 8 years for the highest initial investment cost value of 7000 $/kW for the SOFC. Roy et al. (2019) studied a techno-economic analysis of a system that includes a biomass gasifier, an SOFC, an externally fired gas turbine, and an organic Rankine cycle. The economic analysis results of the system were examined with different operating and design parameters. This study was based on the method proposed by the National Energy Technology Laboratory (NETL). The levelized unit cost of electricity (LUCE) was calculated on a system basis. As a result of the analysis, it was discovered that when current density grows, so does the cost of power, the cost of electricity reduces with the rise in the pressure ratio of the secondary air compressor, and finally, the cost of electricity decreases with the increase in the inlet temperature of the organic vapor turbine (OVT). According to economic analysis, the suggested plant has a minimum levelized unit cost of electricity (LUCE) of 0.086 $/kWh. In a different study, Peng et al. (2021) examined and proposed a hybrid system which consist of WHR subsystem. In this study, cost function and scaling up methods were used. It was found that the hybrid system, which has a modest investment of 29,322.49 k$, delivers high economic effectiveness with a net present value of 109,815.39 k$ during its 20-year life span, and the suggested system has a dynamic payback period of only 3.77 years.

The studies discussed above show that most of these studies are based on exergo-economic analysis. Using this analysis, the specific cost of the useful products and cost flow in hybrid systems were mainly calculated. In these studies, the effects of parameters such as fuel utilization factor, and current density on the total cost were investigated. However, the number of studies examining the effect of component size on the total cost is not sufficient.

There are some studies on the environmental analysis of integrated solid oxide fuel cell and biomass gasifier systems. Some studies in the literature, including the environmental analysis of hybrid systems containing solid oxide fuel cells and biomass gasifiers, are summarized in Table 2.5 with their results. Gholamian et al. (2016) analyzed a trigeneration system having cooling, heating, and power outputs. This system consists of a biomass gasifier, a SOFC, a double effect absorption refrigeration cycle, and HRSG components. In order to evaluate the environmental impact of the system, a simple equation for calculating the CO_2 emission was used. The CO_2 emission values obtained as a result of the study were compared with the CHP (gasifier+SOFC+HRSG) and the system generating only power (SOFC). The CO_2 emission value was found as 56.62 t/MWh in the power generation system, 23.52 t/MWh in the CHP system, and finally 20.37 t/MWh in the trigeneration system. Colpan et al. (2010) worked on two different biomass gasification and SOFC systems. The first configuration includes a dryer, a combustor, an HRSG, a steam turbine, a condenser, and a water pump. The second configuration includes a dryer, a gasifier, a SOFC, an afterburner, an HRSG, and a water pump. Greenhouse gas emissions were calculated for these systems. As a result of this study, it was determined that the GHG emission of the first configuration was higher than the second one. The GHG emission value for the first configuration was found to be 4.564 g-CO_2.eq/Wh and the second configuration as 0.847 g-CO_2eq/W·h. Owebor et al. (2019) worked on a hybrid system including a gasifier, a SOFC, a gas turbine, a steam turbine, an organic Rankine cycle, and an absorption refrigeration cycle. In this study, evaluations were done based on the amounts of CO, CO_2, and NO produced. The values of parameters such as adiabatic flame temperature, holding time, pressure drop in the combustion chamber were investigated on the amounts of these harmful gases produced. As a conclusion, the harmful emission factor was found as 0.009, the sustainability exponent as 5.10, and the specific CO_2 emission as 148.22 kg/MWh CO_2. It was observed that the CO and NO_x emission values increased with the rise in the ratio of the adiabatic flame temperature to the ambient temperature. Likewise, it was observed that the specific CO_2 emission value and the

fuel harmful emission value increased with the increase of the adiabatic flame temperature.

Table 2.5 Studies on the environmental analysis of SOFC and biomass gasifier-based integrated systems (Erdogan et al., 2022)

Study	**Year**	**Components**	**Indicators**	**Results**
Colpan et al. (2010)	2010	Biomass gasifier, SOFC, HRSG	The specific greenhouse gas (GHG) emission	0.847 g-CO_2.eq/Wh
Palomba et al. (2017)	2017	Biomass gasification, SOFC, CHP system	Amount of avoided CO_2 emissions	5000 t/y
Gholamian et al. 2016	2018	Biomass gasifier, SOFC, Double effect absorption refrigeration cycle, HRSG	CO_2 emissions	20.37 t/MWh
Roy et al. (2019)	2019	Biomass gasifier, SOFC, Gas Turbine, ORC	The maximum CO_2 emission reduction potential	3564 t CO_2 /year
Kalina (2019)	2019	Biomass gasifier, SOFC, Internal combustion piston engine, ORC	Specific carbon emission reduction	145.56 kg/GJ_{bio}
Yan et al. (2019)	2019	Biomass gasifier, SOFC, CO_2	The life cycle CO_2 emission	0.591 kg/kWh

CHAPTER THREE
SYSTEM ANALYSIS

3.1 Introduction

Recently, modeling studies on integrated systems that consist of a biomass gasifier and a SOFC have increased. However, the number of studies with different modeling approaches for integrated systems with a biomass gasifier and a SOFC is insufficient. The different modeling approaches studied for the integrated system offer a wider range of interpretations of the system outputs. This section describes in detail the 0-D modeling technique applied to an integrated system having a SOFC and a biomass gasification system.

3.2 System Description

Figure 3.1 depicts the operational system setup. First, biomass enters the gasifier to be gasified, and syngas is formed as a result of this process. This gas has significant levels of tar, sulphur, and other pollutants that may create SOFC degradation problem. As a consequence, based on the SOFC impurity levels, a gas cleaning ought to be used to clean the syngas. The purified syngas is sent into the SOFC, which produces electricity. The syngas and air from the SOFC are burned in the afterburner to raise the temperature of the gas composition. The burning gas is used to raise the temperature of the air supplied by the blower. During air gasification, this gas stream heats both the steam generator and the gasifier. Lastly, the same gas stream heats the drier and is emitted into the atmosphere.

In this study, the gasifier simulation was done through ASPEN Plus program. Gasifier results were transferred to EXCEL program via ASPEN Plus program. With a written code, the EXCEL file was transferred to the 0-D integrated system code,

which was built over MATLAB, and the performance and economic analysis of the system was provided.

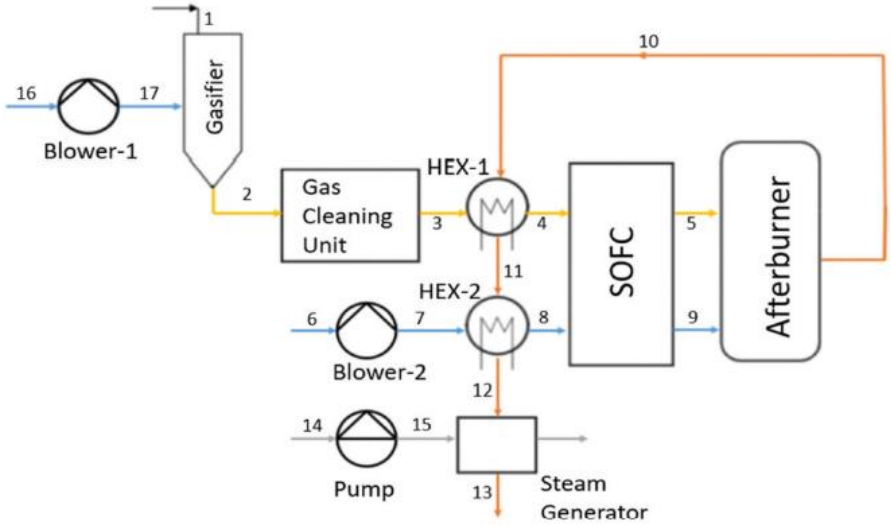

Figure 3.1 Integrated system containing SOFC and biomass gasifier (Erdogan et al., 2022)

3.3 Performance Assessment

By merging the equations of the SOFC, gasifier, and other components, a system-level model for an integrated SOFC and biomass gasifier may be built. In the literature, there are 1-D (Cheddie & Munroe, 2007), 2-D (Audasso et al., 2020; Ni, 2010), and 3-D (Peksen et al., 2013; Sezer et al., 2021) mathematical models for SOFCs. However, coupling these models with the models of other energy systems and using them in the modeling of integrated energy systems is more difficult. The 0-D modeling approach, on the other hand, is favorable in terms of linking the equations and solution time; nevertheless, the results are less accurate. However, the findings are often adequate to assess its performance because the fundamental purpose of system-level modeling is to estimate the value and trend of performance under diverse scenarios.

In the literature, there are many techniques for modeling a gasifier. These techniques are classified based on how they handle processes, such as chemical

kinetics and chemical equilibrium, and how they solve transport equations in different spatial dimensions, such as 0-D (e.g., (Nikoo & Mahinpey, 2008)), 1-D (e.g., (Agu et al., 2019)), 2-D (e.g., (Fletcher et al., 1998)), and 3-D. (e.g., (Baruah & Baruah, 2014; Couto et al., 2013)). The composition of the resultant synthesis gas is computed in a model based on the thermodynamic equilibrium method, assuming that it interacts in a mixed fashion over an endless length of time (Baruah & Baruah, 2014; Puig-Arnavat et al., 2010). Certain reactions are defined in this manner in order to forecast the synthesis gas composition. In the equilibrium approach, the most often utilized approaches are stoichiometric and non-stoichiometric methods (Puig-Arnavat et al., 2010). The stoichiometric approach focuses on the equilibrium constants. It is sufficient to know the proximate analysis values showing the moisture, fixed carbon, and ash content of the biomass and the ultimate analysis values indicating the chemical content in the non-stoichiometric technique. The ultimate and proximate analysis values are important because they can cause considerable variations in the composition of the syngas generated during gasification. The equilibrium method can also be used to minimize the Gibbs free energy (Shabbar & Janajreh, 2013). In a finite process, the kinetic technique is utilized to determine the synthesis gas composition created in the gasifier. The kinetics of gasification processes and the hydrodynamics of the gasifier reactor are significant elements in the kinetic model method. This method is appropriate for usage at low temperatures (Safarian et al., 2019). The distribution of parameters such as species concentration and temperature may be obtained using the computational fluid dynamics (CFD) modeling technique (1-D to 3-D). In the 0-D modeling of the gasifier, an iterative solution approach is commonly employed to identify the syngas composition by applying chemical equilibrium and/or chemical kinetics, atom balances, and energy balance equations. According to studies on gasifier modeling in the literature, the steam-reforming and water-gas shift processes are primarily studied in the modeling. Furthermore, undesirable substances like as tar and ash are commonly overlooked in modeling. The biomass gasification models in the literature are generally created using commercial software such as ASPEN Plus in this method. When this program is utilized, each zone is first developed with distinct built-in reactors, and then the syngas composition is determined.

In this study, the performance analysis of an integrated system with SOFC and gasifier was performed. Firstly, an integrated system with a downdraft gasifier is discussed. The gasifier model constructed with 0-D equilibrium model via ASPEN Plus is based on the stoichiometric approach. Modeling of SOFC and other components based on energy and exergy balances are built on MATLAB in 0-D.

3.3.1 Downdraft Gasifier Modeling

The ASPEN Plus program does not offer a gasifier model as a ready-made package. For this reason, the downdraft gasifier model was constructed using the reactors included in the program. Figure 3.2 presents the modeling of a downdraft gasifier. The biomass first enters the reactor called DRYER(Rstoic) to reduce the moisture content in its content. The calculator named WATERCAL, which works simultaneously with this reactor, makes the necessary calculations for the desired humidity rate. The biomass is then sent to the SEP1 reactor to decompose the unwanted ingredients. In the next step, the biomass is fed into the reactor under the name DECOMP(Ryield) in order to decompose it into its components. Here, a calculator called YIELDCAL is also used to determine the components. The biomass separated into its components is fed into a reactor for gasification. This is a reactor working with the principle of the minimization of the Gibbs free energy model and named as GASIF(Rgibbs). Finally, the synthesis gas formed is fed to the reactor named SEP2 for the separation of the coal, and the synthesis gas is obtained in the designed content.

The following assumptions were made in this modeling of the gasification process:

- A zero-dimensional modeling approach was used.
- The system operates under steady state.
- Particle size is not considered.
- Pressure drops are neglected.
- Heat losses from the reactors are neglected.

- Tar formation is not considered.

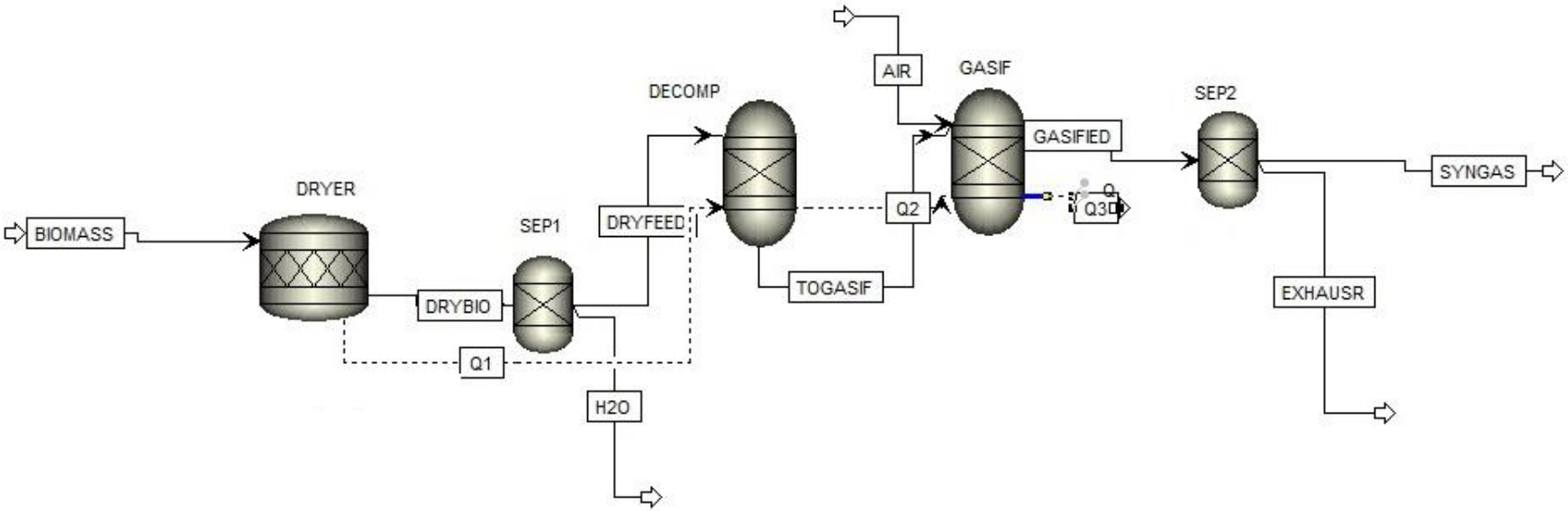

Figure 3.2 ASPEN Plus downdraft gasifier modeling

3.3.2 Components

The components represented in the simulation are listed in Table 3.1 Biomass and ash compositions have been designated as nonconventional solid components due to their ambiguity. Only enthalpy and density for these components were estimated throughout the simulation. For coal-derived materials, special models in Aspen Plus estimate both enthalpy and density. Because biomass is a coal-derived substance, these models may also be used to determine its attributes.

Table 3.1 Component Specifications

Component ID	Type	Component Name
BIOMASS	Nonconventional	-
ASH	Nonconventional	-
C	Solid	CARBON-GRAPHITE
CO2	Conventional	CARBON-DIOXIDE
H2	Conventional	HYDROGEN
CO	Conventional	CARBON-MONOXIDE
CH4	Conventional	METHANE
H2O	Conventional	WATER
N2	Conventional	NITROGEN
O2	Conventional	OXYGEN
S	Conventional	SULFUR
SO2	Conventional	SULFUR-DIOXIDE
HCL	Conventional	HYDROGEN-CHLORIDE
NH3	Conventional	AMMONIA

3.3.3 Physical Properties

The Peng Robinson Boston-Mathias (PK-BM) property was selected as the global property technique for this model. Peng Robinson cubic equation of state with Boston-Mathias alpha function is suitable for non-polar or moderately polar mixtures. For gas processing, refinery, and petrochemical applications, the PK-BM property technique is suggested (Begum et al., 2013).

Biomass and ash were determined as non-traditional components. The simulation model only calculated the density and enthalpy. As shown in Figure 3.3, HCOALGEN was selected for biomass and ash and DCOALIGT was selected for density. HCOALGEN establishes many empirical correlations for the heat of combustion, heat of formation, and heat capacity In this study, option code 1 uses Boie correlation as the calculation method, and option code 6 uses user input value (Technology, 2001).

Figure 3.3 Nonconventional components enthalpy model specifications

The next stage is to find the results of the ultimate, proximate, and sulfur analyses for biomass and ash. The biomass and ash compositions can be found in Table 3.2.

Table 3.2 Biomass and ash compositions based on sulfur, ultimate, and proximate analyses (Tavares et al., 2020)

Ultimate Analysis	**Biomass (wt%)**	**Ash (wt%)**

Carbon	50.6	0

Table 3.2 continues

Oxygen	42	0
Hydrogen	6.5	0
Nitrogen	0.2	0
Sulfur	0	0
Chlorine	0	0
Ash	0.7	100
Proximate Analysis	**Biomass (wt%)**	**Ash (wt%)**
Volatile matter	80.1	0
Fixed Carbon	19.2	0
Ash	0.7	100
Mouisture	20	0

3.3.4 Stream Specification

Table 3.3 shows the parameters for biomass, air, steam, and Q1 as feed streams in the downdraft gasifier model shown in Figure 3.2. Q1 heat refers to the transfer of the reaction heat generated in the dryer model (RStoic) to the RYield reactor for the separation process.

Table 3.3 The inlet streams' specifications

Stream	**Component**	**Temperature (℃)**	**Pressure (atm)**	**Mass flow rate**
BIOMASS	Ultimate and Proximate Analyses	25	1	2000 kg/h
AIR	21% O2 79% N2	800	1	Air to biomass ratio is 1.12

Q1	-	25	-	-

3.3.5 Block Specification

Following the specification of the inlet streams, all of the blocks were defined in accordance with the design operating condition. A summary of the flowsheet's blocks is given in Table 3.4. The precise operating parameters for the blocks are shown in Table 3.5.

Table 3.4 Block Specifications

Aspen plus ID	**Block Name**	**Description**
RStoic	DRYER	Reduces the extra amount of the moisture
Sep	SEP1	Separates remaining moisture from the biogas
RYield	DECOMP	Converts non-conventional biomass into conventional components such as C, H_2, O_2, Cl_2, N_2, and S
RGibbs	GASIF	Calculates the synthesis gas composition by reducing the Gibbs free energy.

Table 3.5 Block Operating Parameters

Block ID	**Temperature (℃)**	**Pressure (atm)**	**Specification**
DRYER	150	1	A calculator block was used to calculate the moisture content.
PYR	25	1	A calculator block was used to calculate the component.
SEP	-	-	A design specification block determined the char split fraction.

GASIFIER	850	1	Determine the phase and chemical equilibrium. The RGibbs model was used to determine the products.

3.3.6 Calculator Specification

Two calculation blocks were used in the downdraft gasifier simulation. The block properties used are explained in this section.

3.3.6.1 Calculator 1

This calculation block is designed for the RYIELD drying system. The calculation block contains a FORTRAN code that calculates the amount of moisture to be removed. The Fortran code that calculates the new moisture content of the biomass is shown in Figure 3.4.

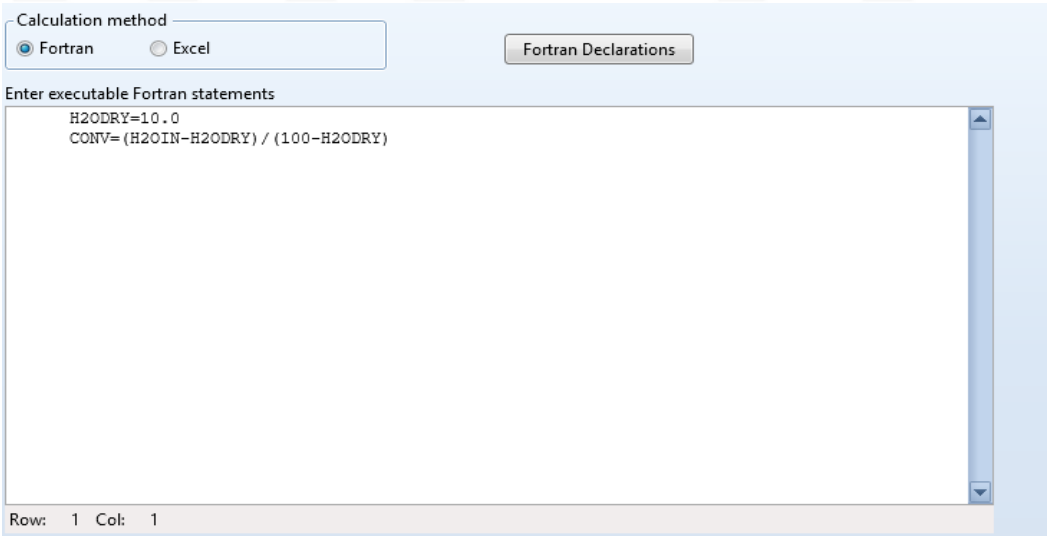

Figure 3.4 Fortran code for drying

3.3.6.2 Calculator 2

Calculator 2 generates the components of the biomass entering the RYield reactor, formed after pyrolysis. Table 4 displays the import variables defined in the Calculator 1 using the category Streams. The Fortran code generated for the pyrolysis process is shown in Figure 3.5 and Figure 3.6.

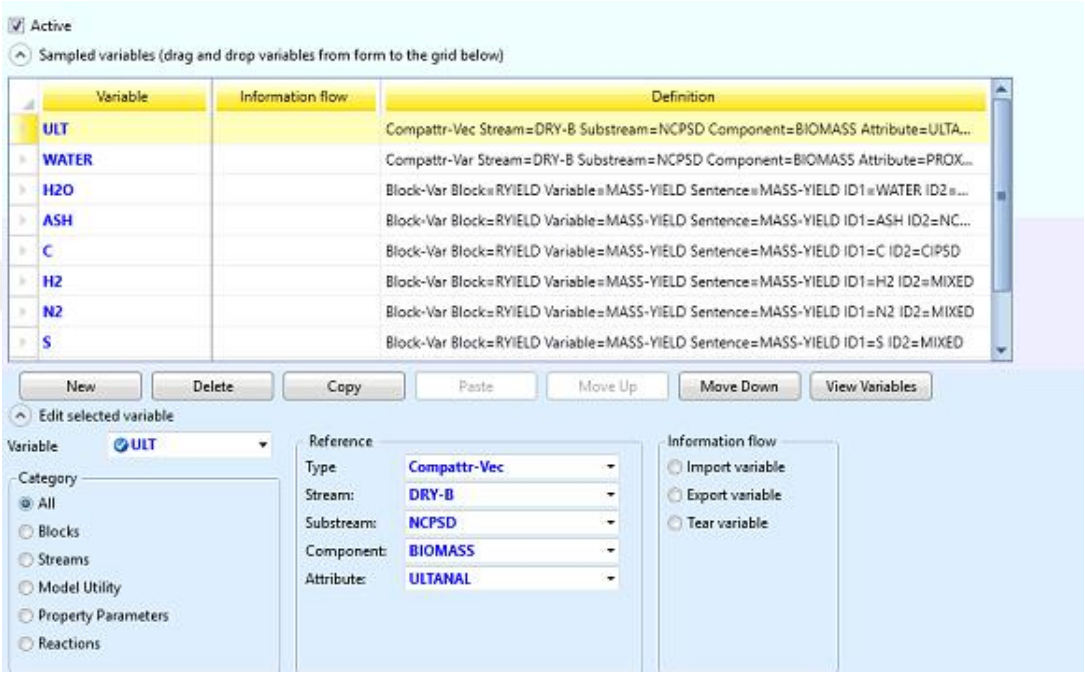

Figure 3.5. Calculator Streams

Figure 3.6 Fortran code for pyrolysis

3.4 SOFC Modeling

SOFC modeling is discussed in this section. In this study, the modeling of SOFC is based on the study of (Colpan et al., 2010). This model is fundamentally based on thermodynamics and electrochemistry. According to the system studied here, 0-D modeling was deemed suitable and was solved in MATLAB.

3.4.1 Basic Calculations

Fuel utilization ratio: It is defined as the ratio of electrochemically reacted hydrogen to the quantity of hydrogen in the incoming stream. It can be calculated as follows (Colpan et al., 2010):

$$FUE = \frac{\dot{N}_{H_2,utilized}}{\dot{N}_{H_2,inlet}} \tag{3.1}$$

Air utilization ratio: It is measured as the fraction of electrochemically reacted oxygen to the total quantity of oxygen in the incoming stream:

$$U_f = \frac{\dot{N}_{O_2,utilized}}{\dot{N}_{O_2,inlet}} \tag{3.2}$$

Electric current, *I*, can be defined as:

$$I = 2\dot{N}_{H_2}F \tag{3.3}$$

F is defined as the Faraday constant and is equal to 96485 C/mol.

Nernst voltage can be defined as:

$$V_{Nernst} = \frac{-\Delta\bar{g}(T_{SOFC})}{2.F} - \frac{R.T_{SOFC}}{2.F}.ln\left(\frac{x_{eq}^{H_2O}}{x_{eq}^{H_2}.\sqrt{x_{eq}^{O_2}.\frac{P_{SOFC}}{P_{ref}}}}\right) \quad (3.4)$$

In Eq.(3.4), T_{SOFC} is solid oxide fuel cell temperature, R universal gas constant, F Faraday constant, $x_{eq}^{H_2O}$, $x_{eq}^{H_2}$ ve $x_{eq}^{O_2}$ respectively, the molar ratio of water, hydrogen and oxygen, P_{SOFC} is the working pressure, and P_{ref} is the reference pressure.

After computing the polarizations, the cell voltage may be calculated as follows:

$$V = V_N - V_{ohm} - V_{act} - V_{con} \quad (3.5)$$

The cell's power output may be calculated as:

$$\dot{W_{FC}} = I.V \quad (3.6)$$

The electrical efficiency of the cell can be obtained as follows:

$$\eta_{el} = \frac{\dot{W}_{net}}{LHV \cdot N_{biomass}} \quad (3.7)$$

3.4.2 Electrochemistry of SOFC

In a solid oxide fuel cell, there are three forms of voltage loss. The barrier to the movement of oxide ions through the electrolyte causes ohmic polarization. The voltage drop generated by the slowness of processes at the electrode-electrolyte interface is known as activation polarization. The barrier to mass transfer between the electrodes and reactant channels is characterized as concentration polarization. These parameters may be determined as follows (Colpan et al., 2010):

$$V_{ohm} = (R_{contact} + \left(\sum_k p_k \,.\, L_k\right).\, i \tag{3.8}$$

$$V_{act} = V_{act,a} + V_{act,c} = \frac{R.T_x}{2.F}.\, sinh^{-1}\left(\frac{i}{2.\, i_{0,a}}\right) + \frac{R.T_x}{F}.\, sinh^{-1}\left(\frac{i}{2.\, i_{0,c}}\right) \tag{3.9}$$

$$V_{conc} = V_{conc,a} + V_{conc,c} = \left[\frac{-R.T_x}{2.F}.\, ln\left(1 - \frac{i}{i_{a,x}}\right) + \frac{R.T_x}{2.F}.\, ln\left(1 + \frac{p^{H2,i}}{p^{H_2O}.i_{c,x}}\right)\right] + \left[\frac{-R.T_x}{4.F}.\, ln\left(1 - \frac{i}{i_{a,x}}\right)\right] \tag{3.10}$$

In these equations, $R_{contact}$ is the contact resistance, p_k is the ionic resistivity of SOFC components, L_k is the thickness of SOFC components, T_x is the surface temperature, $i_{0,a}$ and $i_{0,c}$ are the exchange current densities at the anode and cathode, $i_{a,x}$ and $i_{c,x}$ represent the anode and cathode current density, and $p^{H2,i}$ and p^{H_2O} represent the partial pressure of hydrogen and water.

3.4.3 Exergy Destruction in SOFC

Specific exergy destruction may be defined as follows (Colpan, 2009):

$$e_D = 2 \cdot F\ (V_{ohm} + V_{act} + V_{con}) \tag{3.11}$$

3.5 Thermodynamic modeling of a syngas-fueled SOFCs

The SOFC is simulated using energy balance and electrochemical equations in this study. In the thermodynamic modeling of SOFC, the model approach described by Colpan (2009), in his thesis was applied.

Figure 3.7 depicts the schematic of a unit SOFC. The operating principle of the cell is as follows: The mixture of syngas (state fl) and recirculated gas (state f2) enters the fuel channel (state f3). In the fuel cell, all of the electrochemical processes take place simultaneously. Due to the high-water content of the gases entering the

fuel channel (f4 state), some of them can be recycled to prevent carbon build-up. The remaining fuel leaves the SOFC (state f5). The oxidant passes through the air channel. As the eoxygen molecules in the air react with electrons, the cathode produces oxide ions. The combination of gases containing less oxygen than the incoming air leaves the air duct (state a2). Finally, electron mobility creates an electric current.

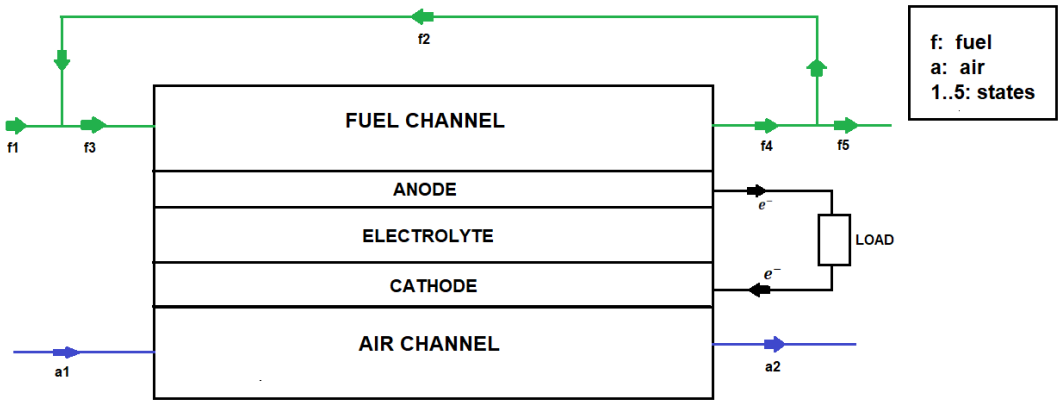

Figure 3.7 SOFC Unit Cell (adapted from Colpan et al., 2008)

3.5.1 Modeling Approach

In modeling, the off-gas composition of the initial gas species primarily determines molar flow rates, recirculation rate, and fuel utilization. The molar flow rate of the hydrogen consumed by the chemical equilibrium equations and the electric current is calculated. The extent of chemical processes and the mass flow rate of the fuel at the inlet are estimated. After determining these variables, the air utilization rate is calculated to solve the energy balance of the fuel cell. Finally, the cell voltage, power output and electrical efficiency are calculated.

The following assumptions were assumed in the analysis (Colpan et al., 2010):

- Syngas composition, i: i = {CH_4, CO_2, CO, H_2O, H_2, N_2}
- Air content is 79% N_2 and 21% O_2 j = {O_2 , N_2}

- Fuel cell is insulated.
- The gas mixture at the fuel channel outlet is chemically balanced.
- Temperature at the channel inlets, and also at the exits is same.
- Fuel cell is operating at steady state.
- Contact resistances are ignored.
- Pressure drops are neglected.

3.5.2 Gas Composition at the Fuel Channel Exit

The fuel channel's equilibrium gas composition may be stated as follows (Colpan et al., 2010):

$$x_{f4,eq}^{CH_4} = \frac{\dot{N}_{f1}^{CH_4} - a}{\dot{N}_{f1} + 2a} \tag{3.12}$$

$$x_{f4,eq}^{H_2} = \frac{\left(\dot{N}_{f1}^{H_2} + 3a + b\right)}{\dot{N}_{f1} + 2a} \cdot \left(\frac{(1-r)(1-U_f}{1 - r + r.U_f}\right) \tag{3.13}$$

$$x_{f4,eq}^{CO} = \frac{\dot{N}_{f1}^{CO} + a - b}{\dot{N}_{f1} + 2a} \tag{3.14}$$

$$x_{f4,eq}^{CO_2} = \frac{\dot{N}_{f1}^{CO_2} + b}{\dot{N}_{f1} + 2a} \tag{3.15}$$

$$x_{f4,eq}^{H_2O} = \frac{\dot{N}_{f1}^{H_2O} + \left(-a - b + \frac{\left(\dot{N}_{f1}^{H_2} + 3a + b\right).U_f}{1 - r + r.U_f}\right)}{\dot{N}_{f1} + 2a} \tag{3.16}$$

$$x_{f4,eq}^{N_2} = \frac{\dot{N}_{f1}^{N_2}}{\dot{N}_{f1} + 2a} \tag{3.17}$$

Here, a, b, and 'f1' are defined as the gas species' molar flow rates and r is the recirculation ratio.

$$r = \frac{\dot{N_{f2}}}{\dot{N_{f4}}} = \frac{\dot{m_{f2}}}{\dot{m_{f4}}} \tag{3.18}$$

The chemical equilibrium equations presented below relate to the processes of water-gas shifting and steam reforming, as well as the relation between the electric charge and the molar flow rate of the hydrogen used.

$$K_{SMR} = \exp\left(\frac{-\Delta\bar{g}}{\bar{R}\cdot T_z}\right) = \frac{\left(x_{f4,eq}^{CO}\right)\cdot\left(x_{f4,eq}^{H_2}\right)^3}{\left(x_{f4,eq}^{CH_4}\right)\cdot\left(x_{f4,eq}^{H_2O}\right)}\cdot {P_{SOFC}}^2 \tag{3.19}$$

$$K_{WGS} = \exp\left(\frac{-\Delta\bar{g}}{\bar{R}\cdot T_Z}\right) = \frac{\left(x_{f4,eq}^{H_2}\right)\cdot\left(x_{f4,eq}^{CO_2}\right)}{\left(x_{f4,eq}^{CO}\right)\cdot\left(x_{f4,eq}^{H_2O}\right)} \tag{3.20}$$

$$I = 2.F.\frac{\left(\dot{N}_{f1}^{H_2} + 3a + b\right)U_f}{1 - r + r.U_f} \tag{3.21}$$

3.5.3 SOFC Output Parameters

The molar flow rates of the gas compositions at the entrance and outflow of the air channel are defined as follows (Colpan et al., 2010):

$$\dot{N}_{a1}^{O_2} = \frac{c}{2.U_{ox}} \tag{3.22}$$

$$\dot{N}_{a1}^{N_2} = \frac{c}{2.U_{ox}}.\frac{79}{21} \tag{3.23}$$

$$\dot{N}_{a2}^{O_2} = \frac{c}{2.U_{ox}} - \frac{c}{2} = \frac{c}{2}\left(\frac{1}{U_{ox}} - 1\right) \tag{3.24}$$

$$\dot{N}_{a2}^{N_2} = \frac{79}{42}.\frac{c}{U_{ox}} \tag{3.25}$$

Where c is defined as:

$$c = \left(\dot{N}_{f3}^{H_2} + 3a + b\right).U_f \tag{3.26}$$

The gas composition at the air channel output is calculated as follows:

$$x_{a2}^{O_2} = \frac{\dot{N}_{a2}^{O_2}}{\dot{N}_{a2}} = \frac{1 - U_{ox}}{100/21 - U_{ox}} \tag{3.27}$$

$$x_{a2}^{N_2} = 1 - x_{a2}^{O_2} \tag{3.28}$$

The enthalpy flow rate can be determined by creating an energy balance around the control volume, by the equation presented below:

$$\dot{H}_{f1} = \sum \dot{N}_{f1}^{i} . \bar{h}^{i}(T_x) = \sum \dot{N}_{f3}^{i} . \bar{h}^{i}(T_y) - \sum \dot{N}_{f2}^{i} . \bar{h}^{i}(T_z) \tag{3.29}$$

For an isolated fuel cell, the energy balance in the vicinity of the fuel cell is written as:

$$\sum \dot{N}_{f1}^{i} . \bar{h}^{i} + \sum \dot{N}_{a1}^{j} . \bar{h}^{j} = \dot{W}_{fc} + \sum \dot{N}_{f5}^{i} . \bar{h}^{i} + \sum \dot{N}_{a2}^{j} . \bar{h}^{j} \tag{3.30}$$

3.6 System Level Modeling

In this part, the energy and exergy balance of an integrated system model is examined. Performance evaluations of these systems are made using electrical efficiency, fuel utilization ratio, and exergetic efficiency values. In addition, the modeling of the integrated system was built in 0-D via MATLAB.

3.6.1 Energy Analysis

According to the first law of thermodynamics, the energy balance applied for a steady state system is as shown in Eq. 3.31 (Colpan et al., 2010):

$$0 = \dot{Q} - \dot{W} + \sum_{i} \dot{m}_i . \dot{h}_i - \sum_{e} \dot{m}_e . \dot{h}_e \tag{3.31}$$

Electrical efficiency and fuel utilization efficiency are some key performance

evaluation parameters for energy systems. Electrical efficiency is shown in Eq. (3.30) and fuel utilization efficiency is shown in Eq. (3.31):

$$\eta_{el} = \frac{\left(\dot{W}_{net}\right)_{plant}}{\dot{\eta}_{fuel}.HV} \tag{3.32}$$

$$FUE = \frac{\left(\dot{W}_{net}\right)_{plant} + \dot{Q}_{useful}}{\dot{\eta}_{fuel}.HV} \tag{3.33}$$

3.6.2 Exergy Analysis

Exergy is the maximum amount of work a system can do to reach mechanical, thermal and chemical equilibrium with its environment. Exergy, unlike energy, is often destructed through irreversibilities inside a system rather than preserved. At steady state, the exergy balance can be calculated as follows (Colpan et al., 2010):

$$0 = \sum_{j}\left(1 - \frac{T_o}{T_j}\right).\dot{Q}_j - \dot{W}_{cv} + \sum_{i}\dot{n}_i.\dot{ex}_i - \sum_{e}\dot{n}_e.\dot{ex}_e - \dot{Ex}_D \tag{3.34}$$

Where ex represents the specific molar flow exergy and $\dot{Ex}_D$ represents the exergy destruction rate. The physical exergy can be calculated as:

$$ex^{PH} = (h - h_o) - T_o(s - s_o) \tag{3.35}$$

Tables can be used to obtain the chemical exergy values of an ideal gas mixture in the literature or its value can be calculated using chemical exergy equation shown below.

$$ex^{CH} = \sum x_k.\overline{ex}_k^{CH} + \bar{R}\,.T_o.\sum x_k.lnx_k \tag{3.36}$$

As shown below, the exergy destruction ratio of a component can be compared to the fuel's exergy rate:

$$y_D = \frac{\dot{E}x_D}{\dot{E}x_F} \tag{3.37}$$

A system's exergetic efficiency can be expressed as:

$$\varepsilon = \frac{\dot{E}x_P}{\dot{E}x_F} = 1 - \frac{\dot{E}x_D + \dot{E}x_L}{\dot{E}x_F} \tag{3.38}$$

3.6.3 Modeling Methodologies and Equations for the Integrated System

In this section, energy and exergy balances are applied to all components of an integrated system mainly consisting of an SOFC and a biomass gasifier. The integrated system can be seen in Figure 3.2.

An energy balance around the afterburner may be used to calculate the specific enthalpy at State 10:

$$\bar{h}_{10} = \frac{\dot{H}_{10}}{\dot{n}_{10,\mathrm{CO_2}} + \dot{n}_{10,\mathrm{O_2}} + \dot{n}_{10,\mathrm{H_2O}} + \dot{n}_{10,\mathrm{N_2}}} \tag{3.39}$$

The specific enthalpy of State 7 may be calculated using an energy balance around heat exchanger as follows:

$$\bar{h}_7 = \bar{h}_6 + \frac{(P_7 - P_6).M_{air}}{\rho_{air}.\eta_{blower}} \tag{3.40}$$

At state 15, specific enthalpy may be expressed as:

$$\bar{h}_{15} = \bar{h}_{14} + \frac{v_{14}(P_{15} - P_{14}).M_{air}}{\eta_{pump}} \tag{3.41}$$

The molar flow rate of steam at State 13 may be computed using an energy

balance around the steam generator as shown below:

$$\dot{n}_{18} = \frac{\dot{H}_{12} - \dot{H}_{13}}{\bar{h}_{18} - \bar{h}_{15}} \tag{3.42}$$

Work inputs for pump and blower may be given as:

$$\dot{W}_{pump} = \dot{n}_{18} \,.\left(\bar{h}_{15} - \bar{h}_{14}\right) \tag{3.43}$$

$$\dot{W}_{blower} = (\dot{n}_{8,O_2} + \dot{n}_{8,N_2}).\,(\,\bar{h}_7 - \bar{h}_6) \tag{3.44}$$

The process's change in enthalpy flow rate may be represented as (Colpan, 2009):

$$\Delta\dot{H}_{process} = \left(\dot{n}_{18} - \dot{n}_{C_xH_yO_z}.\lambda\right).\left(\bar{h}_{18} - \bar{h}_{14}\right) \tag{3.45}$$

Where $\dot{n}_{C_xH_yO_z}$ can be found from Aspen Plus model outputs.

The integrated system's net electrical power may be expressed as:

$$\dot{W}_{net} = \dot{W}_{SOFC} - \dot{W}_{blower} - \dot{W}_{pump} \tag{3.46}$$

Electrical efficiency, fuel utilization efficiency and exergetic efficiency can be described as:

$$\eta_{el} = \frac{\dot{W}_{net}}{\dot{n}_{C_xH_yO_z}.(LHV + m_1.\bar{h}_{fg})} \tag{3.47}$$

$$FUE = \frac{\dot{W}_{net} + \Delta\dot{H}_{process}}{\dot{n}_{C_xH_yO_z}.((LHV + m_1.\bar{h}_{fg})} \tag{3.48}$$

$$\varepsilon = \frac{\dot{W}_{net} + \Delta\dot{E}x_{process}}{\dot{E}x_{C_xH_yO_z} + \dot{n}_{15}.e_{ch,H_2O(l)}} \tag{3.49}$$

Input parameters for the integrated system are as shown in Table 3.6.

Table 3.6 Input parameters for the integrated system (Colpan et al., 2007)

SOFC	
Number of cells in each stack	50
The temperature of the syngas entering the SOFC	800°C
The temperature of the air entering the SOFC	800°C
Cell Pressure	1 atm
Excess air coefficient	7
Recirculation rate	0.1
Active Cell Area	10 x 10 cm^2
Number of repeated elements per single cell	18
Anode thickness	0.05 cm
Electrolyte thickness	0.001 cm
Cathode thickness	0.005 cm
Anode diffusivity	0.91 cm^2 /s
Cathode diffusivity	0.22 cm^2 /s
Other Components	
The temperature of the exhaust gas leaving the system	127°C
Pressure ratio of blowers	1.18
Isentropic efficiency of blowers	0.53
Pressure ratio of the pump	1.2
Isentropic efficiency of the pump	0.8

3.7 Thermoeconomic Analysis

An integrated energy system's economic viability may be assessed by calculating the cost of useful products throughout the plant life and calculating some economic indicators such as the payback period. In such an analysis, carrying charges and expenses should be estimated to find the total revenue requirement. For simplifications, rather than considering the cost variation in each year, levelized costs can be also used. Mainly, thermo-economic and techno-economic analysis methods are used in the cost analysis of integrated energy systems. Thermo-economic analysis combines the principles of economic and thermodynamic analyses (generally exergy analysis). This analysis also referred to as exergo-economic analysis (Ranjan & Kaushik, 2013), can be divided into two categories: cost accounting and optimization-based approaches. Examples of cost accounting approaches are specific exergy costing (SPECO) methodology, exergy cost theory, average cost approach, and last-in-first-out approach (Lozano & Valero, 1993; Torres & Valero, 2021). Thermo-economic functional analysis (Frangopoulos, 1987) and engineering functional analysis (von Spakovsky & Evans, 1993) can be given as examples of economic analysis based on optimization techniques (Lazzaretto & Tsatsaronis, 2006). Techno-economic analysis generally uses a model that couples the output of design and modeling of the energy system with the estimation of capital and operating costs. Several commercial tools, such as HOMER, RETScreen, H2RES, EnergyPLAN, INFORSE, and MARKAL/TIMES (Ma et al., 2018) can be used to find the economic indicators.

In the literature, economic analysis studies for integrated systems have been examined. The exergo-economic analysis method was applied in the economic analysis approach in this study as a consequence of the investigations. The purpose of exergoeconomic analysis is to determine the cost generation period and the cost per unit exergy of a product line. To calculate the unit cost of each exergy stream, a cost balance equation and auxiliary equations are applied to each part in the entire process. The cost balance of a system component for exchanging thermal energy and generating electricity is expressed as (Shayan et al., 2019):

$$\sum \dot{C}_{out,\ k} + \ \dot{C}_{W,\ k} = \ \sum \dot{C}_{in,k} \ + \dot{C}_{q,\ k} + \dot{Z}_{k} \tag{3.50}$$

$$\dot{C} \ = c.\dot{Ex} \tag{3.51}$$

where c denotes the cost per exergy unit, $\dot{Ex}$ is total exergy rate, and $\dot{C}$ is cost rate. Table 3.7 shows the cost functions utilized in the study, which are based on Figure 3.1.

Table 3.7 Cost Functions (Erdogan et al., 2022)

Components	**Cost Functions**	**Cost Balance**	**Auxiliary Equations**
Gasifier	$Z_G = 1600\ x\ (\dot{m}_2)^{0.67}$	$c_1\dot{E}_{x_1} + c_{17}\dot{E}_{x_{17}} + \dot{Z}_{gasifier} = c_2\dot{E}_{x_2}$	$c_1 =$ *a given value*, $c_2 = 0$
HEX-1	$Z_{HEX-1} = 130\ x\ \left(\frac{A_{HEX-1}}{130}\right)^{0.78}$	$c_3\dot{E}_{x_3} + c_{10}\dot{E}_{x_{10}} + \dot{Z}_{HEX-1} = c_4\dot{E}_{x_4} + c_{11}\dot{E}_{x_{11}}$	$c_{10} = c_{11}$
HEX-2	$Z_{HEX-2} = 130\ \left(\frac{A_{HEX-2}}{130}\right)^{0.78}$	$c_7\dot{E}_{x_7} + c_{11}\dot{E}_{x_{11}} + \dot{Z}_{HEX-2} = c_8\dot{E}_{x_8} + c_{12}\dot{E}_{x_{12}}$	$c_{12} = c_{11}$
SOFC stack	$Z_{SOFC} = A_{cell}N_{cell}(2.9T_{cell} - 1907)$	$c_4\dot{E}_{x_4} + c_8\dot{E}_{x_8} + \dot{Z}_{SOFC} = c_5\dot{E}_{x_5} + c_9\dot{E}_{x_9} + C_P\dot{W}_{SOFC}$	$c_5 = c_9$
Afterburner	$Z_{AB} = \left(\frac{46.08\ x\ \dot{m}_{air\ pre-heater}}{0.995 - P_{out}/P_{in}}\right)[1 + exp(0.018T_{AB}) - 26.4]$	$c_5\dot{E}_{x_5} + c_9\dot{E}_{x_9} + \dot{Z}_{AB} = c_{10}\dot{E}_{x_{10}}$	N/A
Steam Generator	$Z_{SG} = 130\ \left(\frac{A_{SG}}{130}\right)^{0.78}$	$c_{12}\dot{E}_{x_{12}} + c_{15}\dot{E}_{x_{15}} + \dot{Z}_{SG} = c_{13}\dot{E}_{x_{13}} + c_{steam}\dot{E}_{x_{steam}}$	$c_{12} = c_{13}$

Table 3.7 continues

Blower-1	$Z_{Blower-1} = 91562 \left(\frac{\dot{W}_{blower-1}}{455}\right)^{2/3}$	$c_{16}\dot{E}_{x_{16}} + c_{blower}\dot{W}_{blower} + \dot{Z}_{blower} = c_{17}\dot{E}_{x_{17}}$	N/A
Blower-2	$Z_{Blower-2} = 91562 \left(\frac{\dot{W}_{blower-2}}{455}\right)^{2/3}$	$c_{6}\dot{E}_{x_{6}} + c_{blower}\dot{W}_{blower} + \dot{Z}_{blower} = c_{7}\dot{E}_{x_{7}}$	N/A

3.8 Environmental Analysis

Environmental analysis of an integrated SOFC and downdraft gasifier system is done to evaluate the environmental impact mainly for the following problems: deforestation, land degradation, water pollution, air pollution, and climate change (Sansaniwal et al., 2017). Two main techniques, which are exergo-environmental analysis and life cycle assessment, are used for this purpose. The CO_2 emission value formulas used in the exergo-environmental analysis method are given as follows for the SOFC and CHP system. Approaches that combine the concepts of exergy and environmental assessment can be given as cumulative exergy consumption, exergoecological analysis, extended exergy accounting, and environomic method. However, these approaches do not include the life cycle of the components. In the life cycle assessment, emission values and consumption for each material stream during all processes within the life cycle are analyzed (MEYER et al., 2009).

Another way to evaluate integrated systems from an environmental perspective is to calculate greenhouse gas emissions (GHG) from the system. Examples of greenhouse gases can be given as CO_2, CH_4, and N_2O. The GHG emission value can be calculated as follows:

$$\sigma = \frac{\dot{m}_{GHG}}{\dot{W}_{net,system}} \tag{3.52}$$

$\dot{m}_{GHG}$ indicates the flow rate of the greenhouse gas and $\dot{W}_{net,system}$ indicates the total power of the system. In terms of energy and the environment, the smaller the ratio is, the more ecologically beneficial the system is (Colpan et al., 2009).

CHAPTER FOUR
RESULTS AND DISCUSSION

4.1 Introduction

The findings and discussion of the modeling studies are provided under several sub-titles in this section. First, the findings of the 0-D analysis of the downdraft gasifier type are given. The change of the syngas composition with the gasifier temperature is first shown. Then, the performance evaluation of the integrated system with a downdraft gasifier is conducted through 0-D modeling. For the performance evaluation of the integrated system, energy and exergy balances are applied for each component of the system. As a result of the study, the effects of gasifier temperature and current density on the electrical efficiency, power value, exergy efficiency, fuel utilization efficiency (FUE), and exergy destruction values of the integrated system are assessed. To find the cost of the products, the exergo-economic analysis presented in chapter 2 is applied. The cost functions described in Table 3.7 and the exergy flow values are used. The economic evaluation is based on the integrated system with a downdraft gasifier and SOFC. The effects of gasifier temperature, SOFC stack number, and biomass cost on the cost of produced electricity are investigated. Finally, environmental analysis was applied to the system which includes a downdraft gasifier and a SOFC. GHG emission values were calculated using the greenhouse gas molar flow rates Eq. (3.54) obtained as a result of the 0-D modeling of the system.

4.2 Model Validation

In this study, the model built on ASPEN Plus for the downdraft gasifier and the MATLAB model for the SOFC have been validated by various studies in the literature.

4.2.1 Validation of the Downdraft Gasifier Model

The ASPEN Plus model used for the downdraft gasifier was compared with the results of the study of Tavares et al. (2020). Synthesis gas molar ratios were found to be quite compatible, except for CH_4. The reason for the difference in the methane molar fraction can be attributed to the high-temperature operation of the RGibbs reactor. A detailed explanation of this subject can be found in the work of (Liu et al., 2016). As can be seen in Table 4.1, the difference between the results obtained from the model and those obtained from the study in the literature were found in the range of 4%-13%.

Table 4.1 Validation results of downdraft gasifier

Chemical species	**Molar fractions (Tavares et al., 2020)**	**Molar fractions (Current model)**
Methane	0.02	0.09
Hydrogen	0.15	0.17
Carbon monoxide	0.20	0.21
Carbon dioxide	0.13	0.09
Nitrogen	0.50	0.44

4.2.2 Validation of SOFC Model

The MATLAB model created for SOFC was compared with the results of Colpan et al. (2007). The difference between the results from the SOFC model and the reference study was calculated between 3% and 7%. The reason for the error can be explained by using two different programs and different solution algorithms for SOFC modeling.

Table 4.2 Validation results of SOFC

Current density (A/cm^2)	**Cell voltage of the model (V)**	**Cell voltage found in the study of Colpan et al. (2007) (V)**
0.1	0.880	0.830
0.2	0.765	0.794
0.3	0.731	0.753
0.4	0.718	0.705
0.5	0.673	0.639
0.6	0.610	0.570

4.3 Performance Assessment Results

In this section, performance analysis of integrated systems was done in MATLAB. FUE, exergy efficiency, and SOFC power values, which determine the performance values for the integrated system, are discussed. Parametric studies were carried out using MATLAB with the equations described in Chapter 2. The effects of gasifier temperature and current density were investigated with parametric studies.

4.3.1 Gasification Simulation Results

In this section, the results of the 0-D downdraft gasifier analysis performed over the ASPEN Plus program are given. The change in synthesis gas composition and its LHV value with the gasifier temperature were investigated parametrically.

4.3.1.1 The Effect of Gasifier Temperature on the Molar Fraction of Syngas

Figure 4.1 shows the effect of gasifier temperature on the molar fractions of hydrogen and carbon monoxide. As the gasifier temperature increases, hydrogen and carbon monoxide molar fractions increase. As the gasifier temperature increases, the

molar fraction of methane and carbon dioxide decreases. The highest carbon monoxide value was 0.23 at 900°C s, the hydrogen value was 0.19 at 670 °C, and the carbon dioxide value was 0.15 at 600°C. Chemical processes occurring in the gasifier during the operation can explain these tendencies. Gasification at higher temperatures promotes the production of endothermic and exothermic products and reactants. The methane steam reforming, water gas shift, and Boudouard reactions are shown in Chapter 3, Table 2.2. As a result, when the temperature increases, more CO_2 and CH_4 are converted, and the mole percentage of CO and H_2 increases in proportion to the temperature rise (Basu, 2010). Furthermore, in exothermic processes (such as methanation), equilibrium begins to shift to the left, creating less CO_2 and CH_4, which adds to a decrease in CO_2 and CH_4 ratios. The generation of CO and H_2 in both gasification processes hits a plateau after the gasification temperature of around 1050 K due to gasifying agent depletion, and therefore reactions approach an equilibrium condition. Beyond a given gasifier temperature, no significant CO and H_2 change production is seen due to the absence of gasifying medium (oxygen) ratios (Basu, 2010).

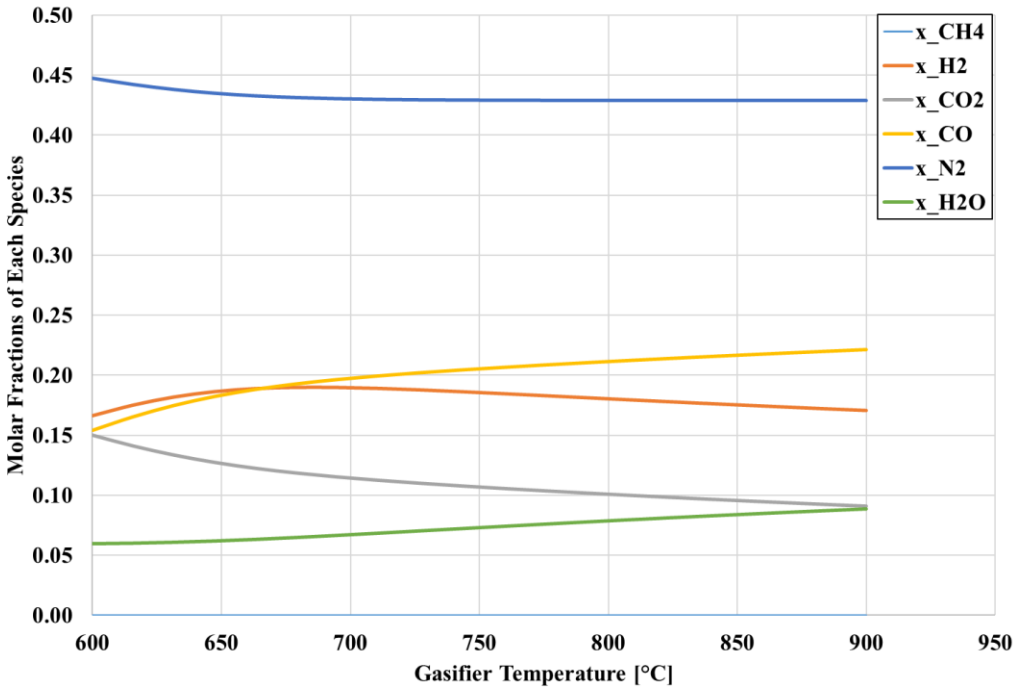

Figure 4.1 Effect of gasifier reactor temperature on the molar fractions of syngas

4.3.1.2 The Effect of Gasifier Temperature on the Lower Heating Value (LHV) of Syngas

Figure 4.2 shows the change in LHV of the syngas with the gasifier temperature. It is observed that the LHV of syngas increases depending on the gasifier temperature between 600-900°C. LHV of syngas, which reaches about 5.45 MJ/m^3 at 600°C, rises to 5.71 MJ/m^3 at 900°C. The LHV of producing gas increases as the temperature of the gasifier rises. Because endothermic chemical processes such as Bouduoard, steam methane reforming and water-gas shift reactions are preferred at higher temperatures, they create more CO and H_2, which contribute significantly to the LHV of the producing gas.

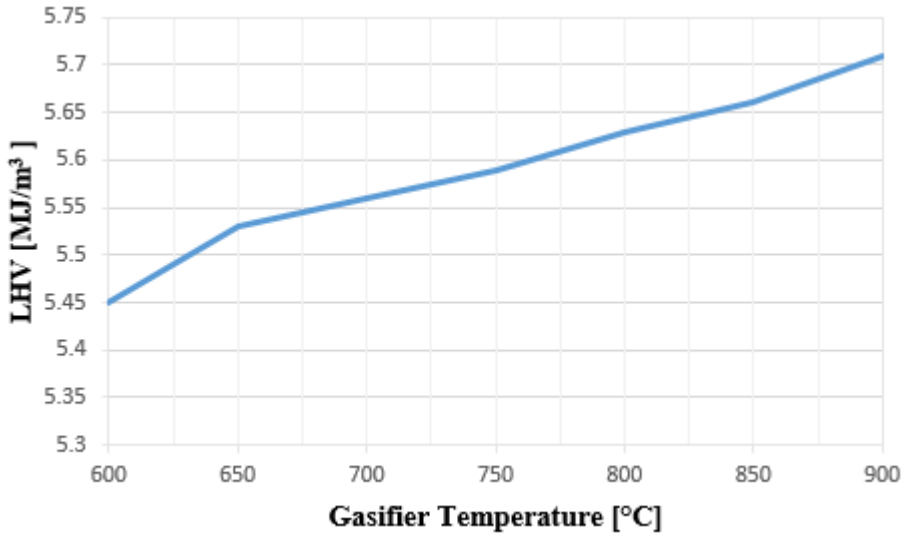

Figure 4.2 The change of LHV of the syngas depending on the gasifier temperature

4.3.2 SOFC Modeling Results

In this section, the change of power density and voltage value with the changing current density values of the SOFC model created on MATLAB is examined.

4.3.2.1 The Effect of Current Density on Cell Voltage and Power

During the operation of the fuel cell, activation, concentration, and ohmic losses occur. The ohmic, activation, and concentration losses are calculated using Eqs. (3.8)-(3.10), respectively. As expected, these losses cause a decrease in cell voltage as current is drawn. The fuel cell power values can also be seen in Figure 4.6. The increasing current density value caused the power value of the fuel cell to increase. The SOFC model with an active area of 100 cm^2 and 50 stacks reached a current density of 1.2 A/cm^2 and the highest power value of 66 kW. However, at this current density, the cell voltage reached its lowest value of 0.48 V.

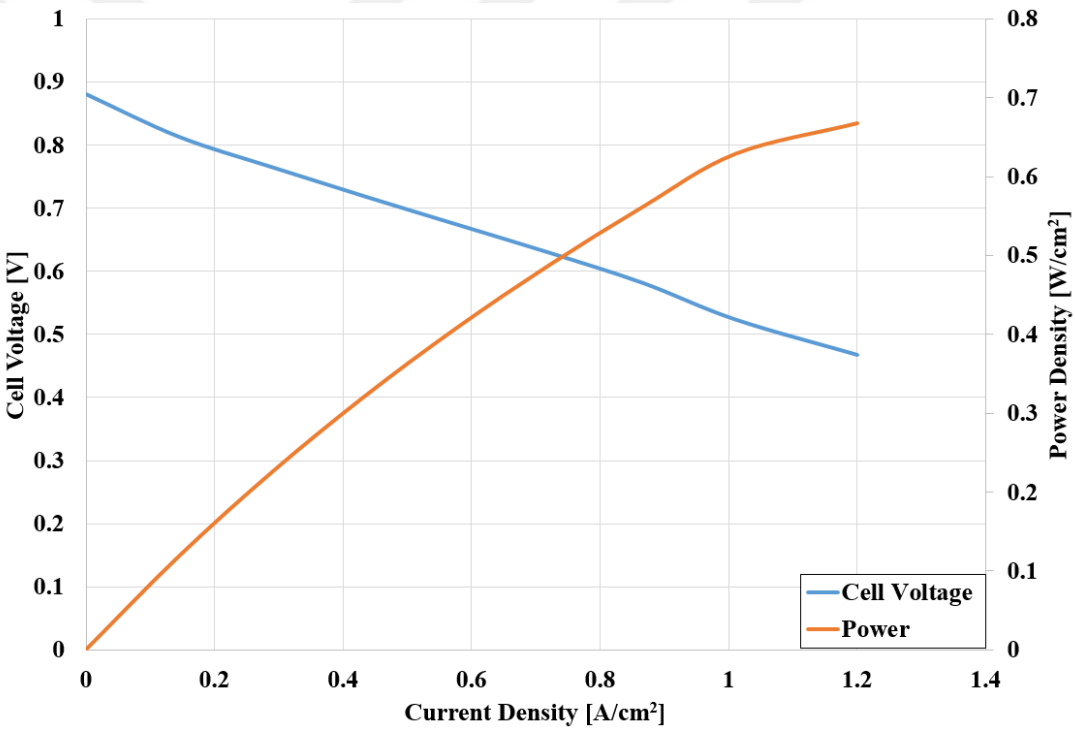

Figure 4.3 The polarization curve for different current density values

4.3.3 System Level Modeling Results

In this section, the syngas results from the downdraft gasifier are transferred to MATLAB via EXCEL, and the exergy efficiency of the integrated system, FUE, and exergy destruction of each component are parametrically examined.

4.3.3.1 The Effect of Gasifier Temperature on Electrical Efficiency, Fuel Utilization Efficiency, and Exergy Efficiency

The effect of gasifier temperature on electrical efficiency and fuel utilization efficiency is depicted in Figure 4.4. In this graph, the electrical efficiency was obtained using Eq. (3.47). At high temperatures of the syngas, the Nernst voltage increases, and accordingly the SOFC stack voltage increases. This change causes an increase in the net power of the system. For this reason, the electrical efficiency of the system increases. However, when the gasifier temperature increases, the fuel utilization efficiency, shown in Eq. (3.48), decreases due to a decrease in usable heat from the steam. Furthermore, it can be seen that increasing the gasifier temperature from 800°C to 980°C reduces electrical efficiency by 7.69% while decreasing FUE by 22.5%.

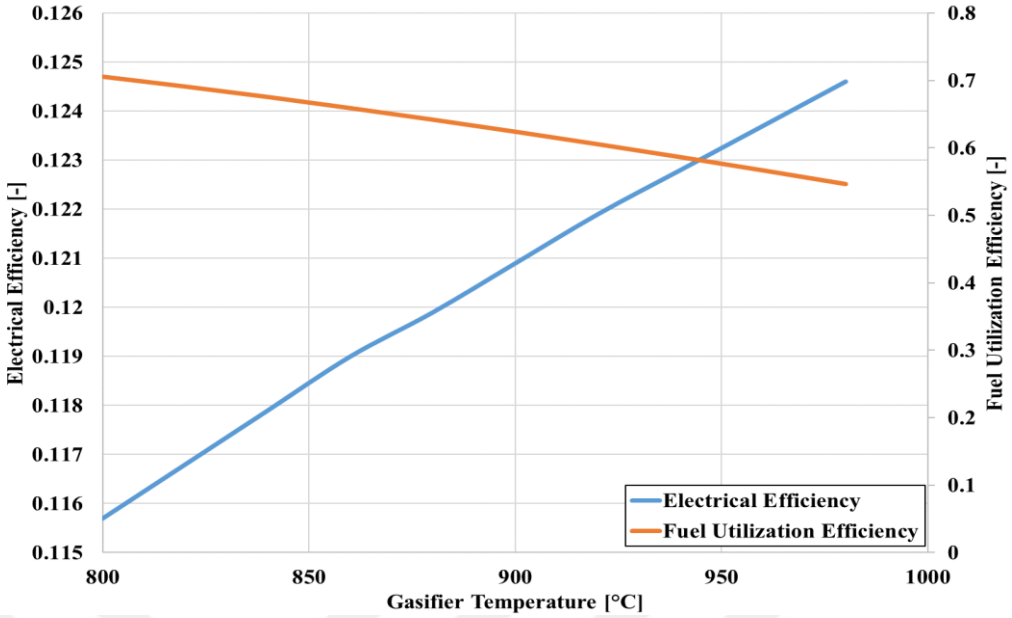

Figure 4.4 The effect of gasifier temperature on electrical efficiency and fuel utilization

Figure 4.5 shows the changes in exergy efficiency values with gasifier temperature. Eq. (3.49) was used to determine the exergy efficiency value. When the gasifier temperature rises, the integrated system's exergy efficiency falls. At high temperatures, the exergy value tends to decrease depending on the increase in the entropy of the system, and accordingly, the exergy efficiency value decreases. When the gasifier temperature was 700°C, the exergy efficiency was found to be 32%.

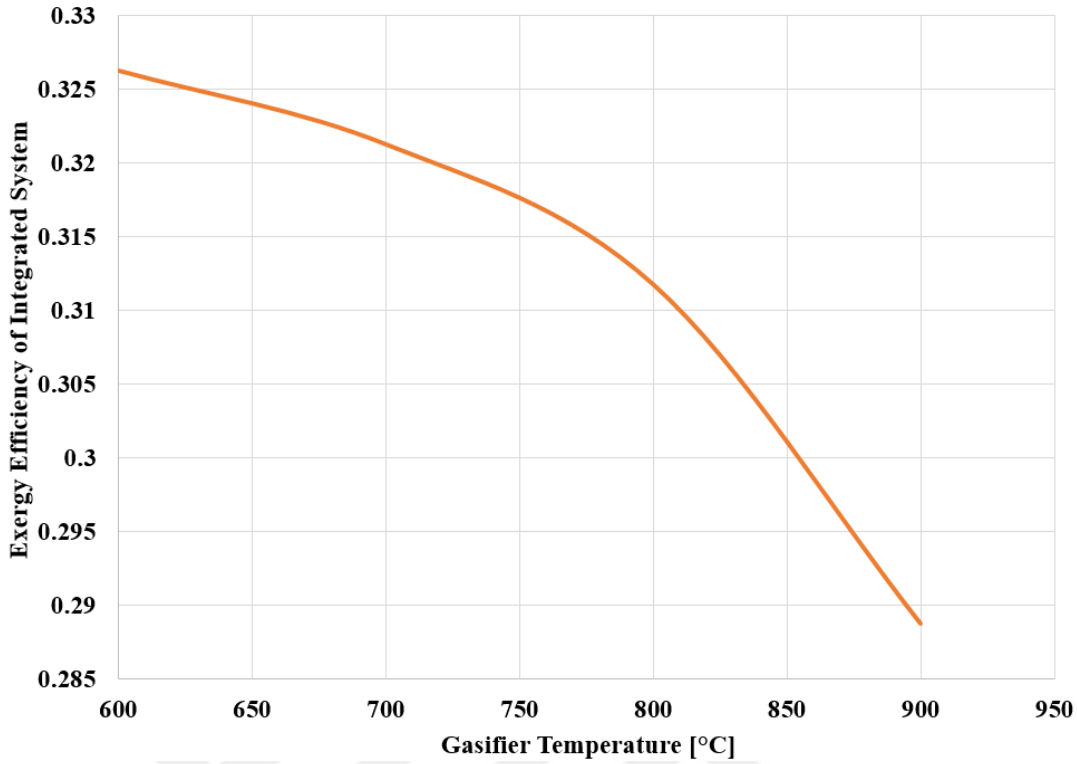

Figure 4.5 Change in exergy efficiency values with gasifier temperature

4.3.3.2 The Effect of Gasifier Temperature on Exergy Destruction of Each Component

Figure 4.6 shows the effect of gasifier temperature on the exergy destruction of each component. As shown in this figure, the exergy destruction value increased in the gasifier and solid oxide fuel cell as the gasifier temperature increased, while the opposite trend was observed in the other components. This is due to a large number of chemical reactions taking place in the solid oxide fuel cell and gasifier (Shayan et al., 2019). The exergy destruction rates in the other components are significantly lower than those in SOFC and gasifier. While the exergy destruction value reaches 1600 W in the gasifier at 900 °C, the exergy destruction value for SOFC reaches approximately 800 W at this temperature.

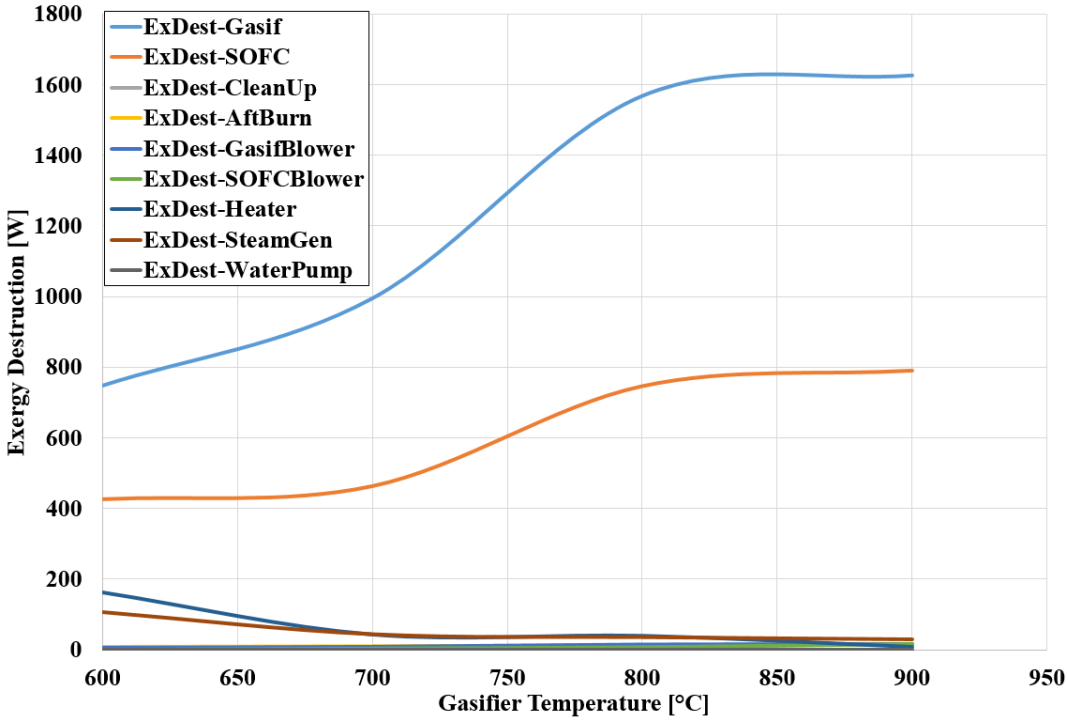

Figure 4.6 The effect of gasifier temperature change on the exergy destruction rate

4.4 Thermoeconomic Analysis Results

In this section, the thermoeconomic analysis of an integrated system with a downdraft gasifier and SOFC is evaluated. First, exergy calculations were made for each component of the system via MATLAB. Then, based on Eq. (3.50), the thermoeconomic analysis results of the system were examined by using the cost functions shown in Table 3.7.

4.4.1 The Effect of Gasifier Temperature on the Produced Electricity of the System

Figure 4.7 depicts the influence of gasifier temperature on the system's cost of generated power. The SOFC power value increases as the gasifier temperature rises, as does the quantity of hydrogen in the syngas content supplied to the SOFC. The

cost of generated electricity rises in direct proportion to the amount of power produced by SOFC.

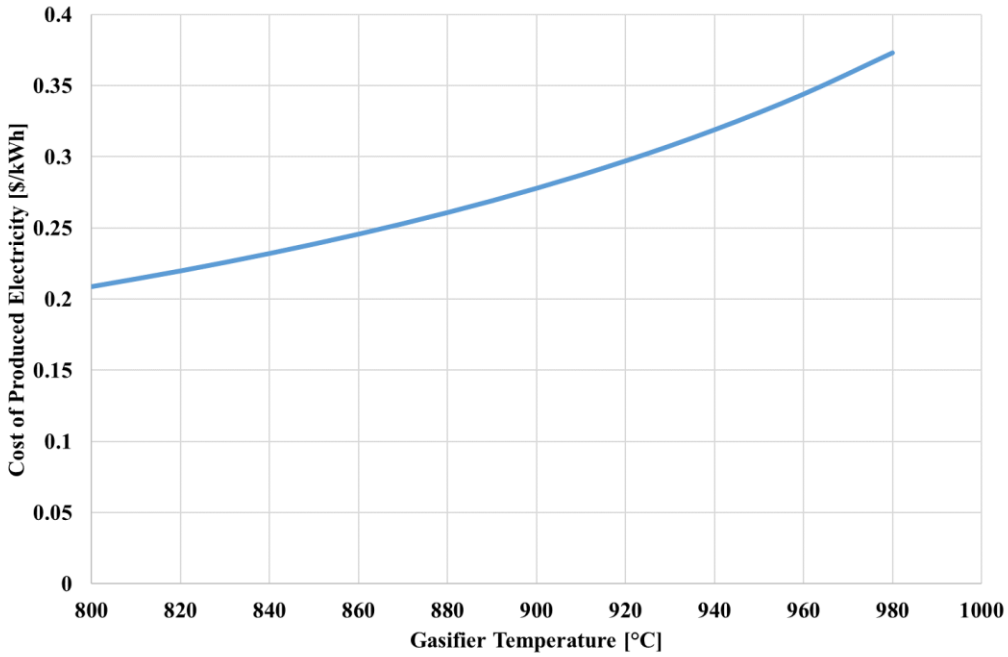

Figure 4.7 The effect of gasifier temperature on the cost of produced electricity

4.4.2 The Effect of Biomass Price on Cost of Produced Electricity

The influence of biomass pricing on the cost of generated power is depicted in Figure 4.8. In Chapter 3, cost functions are given in Table 3.7 for the thermoeconomic analysis method. Exergy balances are established for each component. The c_1 value is defined for the biomass cost fed to the gasifier. Accordingly, with the increase of c_1 value (biomass price) in the equation established for the gasifier, the cost of produced electricity value of the system also increases.

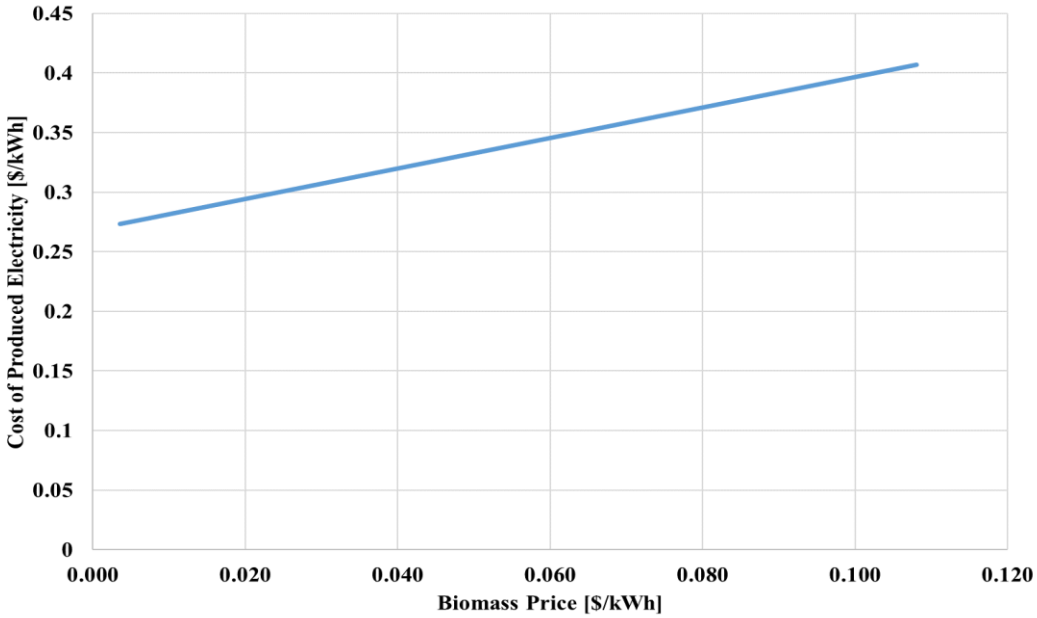

Figure 4.8 The influence of biomass pricing on the cost of produced electricity

4.4.3 The Effect of Number of SOFC Stacks on the Cost of Produced Electricity

Figure 4.9 depicts the influence of the number of SOFC stacks on the cost of power produced. The SOFC output power is given in Eq. (3.6). Accordingly, an increase in the stack number of SOFCs causes an increase in produced power value. It is observed that the cost of produced electricity value also increases with the increasing power value. However, it should be noted that this parameter might be optimized to improve system performance while lowering costs.

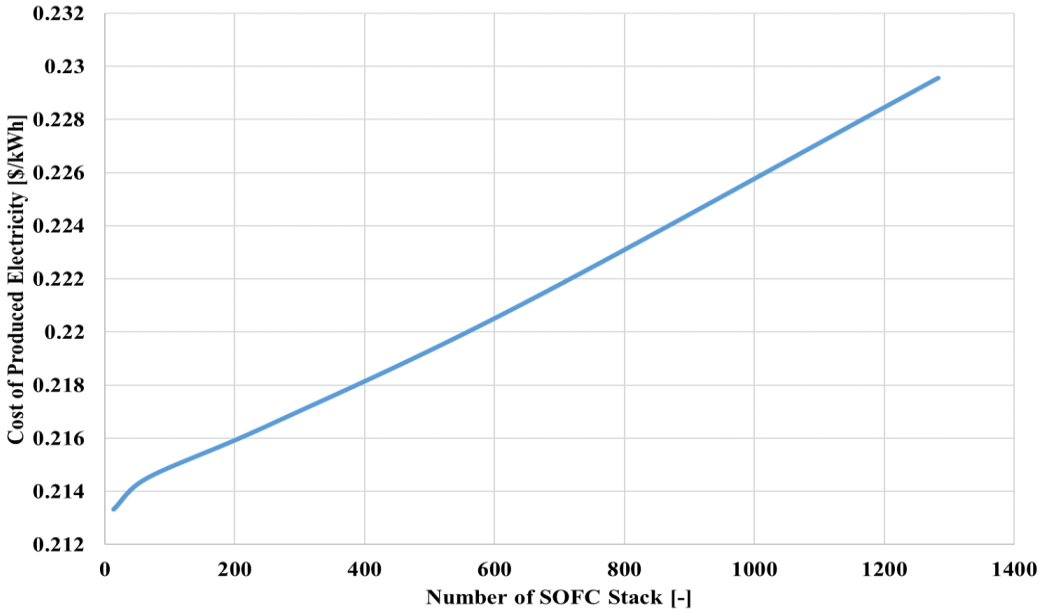

Figure 4.9 The effect of number of SOFC stacks on the cost of produced electricity

4.5 Environmental Analysis

As the last part of the study, environmental analysis of an integrated system with a downdraft gasifier and SOFC was considered. Firstly, the afterburner output molar flow rate is obtained for CO_2. In the next step, the molar flow rate was converted to the mass flow rate. Finally, the greenhouse gas emission value was found as 0.512 g.CO_2.eq/Wh by dividing the mass flow rate by the net system power output as explained in Eq. (3.52).

In a study conducted by Colpan et al. (2009), GHG emission values were obtained for different power generation systems such as internal combustion engine, gas turbine, SOFC, and SOFC-containing cogenerative systems. As a result of the study, the lowest GHG emission value was obtained in the cogenerative system containing SOFC and was found to be 1.12 tonnes CO_2.eq/Wh. In light of the studies carried out, SOFC seems to be the most suitable option from a variety of technologies.

CHAPTER FIVE
CONCLUSIONS

Integrated systems containing a SOFC and a gasifier are promising power-producing systems due to their high efficiency and low emission values. In this thesis, the performance of these systems is first evaluated by the mathematical modeling technique. For this purpose, a 0-D gasifier model, a 0-D SOFC model, and a system-level model based on energy and exergy analysis are conducted. The effects of gasifier temperature (600-1000°C) and current density (0-1.4 A/cm^2) on the performance were investigated. In addition to the thermodynamic modeling of the system, the economic and environmental analyses of these systems were examined and discussed. In the economic analysis study, the effects of gasifier temperature, SOFC stack number, and biomass price parameters were examined. Finally, from an environmental point of view, the GHG emission value of the integrated system is calculated.

The main findings as a result of the analyzes made for the downdraft gasifier and SOFC are as follows:

- When the gasifier temperature increases, the molar fraction of carbon monoxide and hydrogen increases. On the other hand, the molar fraction of hydrogen first increases until the temperature is around 720°C, and then decreases. At 900 ℃it is observed that the highest molar fraction of carbon monoxide was 0.23, the highest value for that of hydrogen was 0.19, and the highest value for that of carbon dioxide was 0.15.
- The LHV of syngas rises with gasifier temperatures ranging from 600 to 900°C. Syngas LHV rises from around 5.45 at 600°C to 5.71 at 900°C.
- The SOFC power was found to be 66 kW and the cell voltage was 0.48 V at 1.2 A/cm^2 current density.

Secondly, a 0-D analytical model of an integrated system with a downdraft gasifier and SOFC was developed. In the analyzes made, the effects of gasifier temperature, SOFC power, and current density on electrical efficiency, exergy efficiency, FUE, exergy destruction rate, and fuel cell power were parametrically investigated. The main findings as a result of the performance analyses made for the integrated system which contains a downdraft gasifier and an SOFC are as follows:

- When the gasifier temperature rises, the integrated system's exergy efficiency falls. At high temperatures, the exergy value tends to drop as the entropy of the system increases, and therefore the exergy efficiency value decreases. The exergy efficiency was determined to be 32% when the gasifier temperature was 700°C.
- While the electrical efficiency was roughly 12.3% at the gasifier temperature of 930°C, the fuel utilization efficiency was calculated as 57%.
- It was obtained from the study that at the baseline conditions the highest exergy destruction value is 1600 W at 900°C in the gasifier, whereas the lowest exergy destructions are in the pump and gas cleaning unit.

Thirdly, the effect of gasifier temperature, SOFC power, and biomass price on the cost of produced electricity is investigated. The main findings as a result of the thermoeconomical and environmental analyses made for the integrated system are as follows:

- As the gasifier temperature rises, the cost of the produced electricity increases. The cost of produced electricity value at 900°C was found to be 0.28 $/kWh.
- As the SOFC power increases, the cost of produced electricity increases. At 900°C, the cost of produced electricity value was found as 0.228 $/kWh.
- It is observed that the as biomass price increases, the electricity cost increases. At 0.060 $/kWh value of biomass price, the cost of produced electricity value was found as 0.34 $/kWh.

- From an environmental point of view, the CO_2 emission value of the integrated system was found to be 0.512 g.CO_2.eq/Wh.

REFERENCES

Abdelkareem, M. A., Elsaid, K., Wilberforce, T., Kamil, M., Sayed, E. T., & Olabi, A. (2021). Environmental aspects of fuel cells: A review. *Science of The Total Environment*, *752*, 141803.

Abuadala, A., & Dincer, I. (2011). Exergoeconomic analysis of a hybrid system based on steam biomass gasification products for hydrogen production. *International Journal of Hydrogen Energy*, *36*(20), 12780–12793.

Administration, U. . E. I. (2022). *Energy Information Administration*. https://www.eia.gov/energyexplained/biomass/

Agu, C. E., Pfeifer, C., Eikeland, M., Tokheim, L.-A., & Moldestad, B. M. E. (2019). Detailed One-Dimensional Model for Steam-Biomass Gasification in a Bubbling Fluidized Bed. *Energy & Fuels*, *33*(8), 7385–7397.

Audasso, E., Bianchi, F. R., & Bosio, B. (2020). 2D Simulation for CH4 Internal Reforming-SOFCs: An Approach to Study Performance Degradation and Optimization. *Energies*, *13*(16), 4116.

Bang-Møller, C., & Rokni, M. (2010). Thermodynamic performance study of biomass gasification, solid oxide fuel cell and micro gas turbine hybrid systems. *Energy Conversion and Management*, *51*(11), 2330–2339.

Barbir, F. (2005). *PEM Fuel Cells*. Elsevier. https://doi.org/10.1016/B978-0-12-078142-3.X5000-9

Baruah, D., & Baruah, D. C. (2014). Modeling of biomass gasification: A review.

Renewable and Sustainable Energy Reviews, *39*, 806–815.

Basu, P. (2010). *Biomass Gasification and Pyrolysis* (1st ed.).

Begum, S., Rasul, M., Akbar, D., & Ramzan, N. (2013). Performance Analysis of an Integrated Fixed Bed Gasifier Model for Different Biomass Feedstocks. *Energies*, *6*(12), 6508–6524.

Carrette, L., Friedrich, K. A., & Stimming, U. (2000). Fuel Cells: Principles, Types, Fuels, and Applications. *ChemPhysChem*, *1*(4), 162–193.

Cheddie, D. F., & Munroe, N. D. H. (2007). A dynamic 1D model of a solid oxide fuel cell for real time simulation. *Journal of Power Sources*, *171*(2), 634–643.

Choudhury, H. A., Chakma, S., & Moholkar, V. S. (2015). Biomass Gasification Integrated Fischer-Tropsch Synthesis. In *Recent Advances in Thermo-Chemical Conversion of Biomass* (pp. 383–435). Elsevier.

Colpan, C. Ozgur. (2009). *Thermal Modeling of Solid Oxide Fuel Cell Based Biomass Gasification Systems*. Carleton University.

Colpan, C. Ozgur, Dincer, I., & Hamdullahpur, F. (2008). A review on macro-level modeling of planar solid oxide fuel cells. *International Journal of Energy Research*, *32*(4), 336–355.

Colpan, C. Ozgur, Dincer, I., & Hamdullahpur, F. (2009). The reduction of greenhouse gas emissions using various thermal systems in a landfill site. *International Journal of Global Warming*, *1*(1/2/3), 89.

Colpan, C. Ozgur, Hamdullahpur, F., Dincer, I., & Yoo, Y. (2010). Effect of gasification agent on the performance of solid oxide fuel cell and biomass gasification systems. *International Journal of Hydrogen Energy*, *35*(10), 5001–5009.

Colpan, C.O., Dincer, I., & Hamdullahpur, F. (2007). Thermodynamic modeling of direct internal reforming solid oxide fuel cells operating with syngas. *International Journal of Hydrogen Energy*, *32*(7), 787–795.

Colpan, C Ozgur, Hamdullahpur, F., & Dincer, I. (2010). *Solid Oxide Fuel Cell and Biomass Gasi cation Systems for Better Efficiency and Environmental Impact Solid Oxide Fuel Cell and Biomass Gasification Systems for Better Efficiency and Environmental Impact*. *78*.

Colpan, Can O., Nalbant, Y., & Ercelik, M. (2018). 4.28 Fundamentals of Fuel Cell Technologies. In *Comprehensive Energy Systems* (pp. 1107–1130). Elsevier.

Couto, N., Silva, V., Monteiro, E., Brito, P. S. D., & Rouboa, A. (2013). Experimental and Numerical Analysis of Coffee Husks Biomass Gasification in a Fluidized Bed Reactor. *Energy Procedia*, *36*, 591–595.

Ebrahimi, M., & Moradpoor, I. (2016). Combined solid oxide fuel cell, micro-gas turbine and organic Rankine cycle for power generation (SOFC–MGT–ORC). *Energy Conversion and Management*, *116*, 120–133.

Energy Information Administration, U. (2019). *Annual Energy Outlook 2019 with projections to 2050*. www.eia.gov/aeo

Erdogan, A., Dursun, B., Colpan, C. O., & Ayol, A. (2022). A review on performance, economic, and environmental analyses of integrated solid oxide fuel cell and biomass gasification systems. *Energy Sources, Part A: Recovery, Utilization, and Environmental Effects*, *44*(4), 8403–8426.

Fletcher, D. F., Haynes, B. S., Chen, J., & Joseph, S. D. (1998). Computational fluid dynamics modelling of an entrained flow biomass gasifier. *Applied Mathematical Modelling*, *22*(10), 747–757.

Frangopoulos, C. (1987). Thermo-economic functional analysis and optimization. *Energy*, *12*(7), 563–571.

Ghaffarpour, Z., Mahmoudi, M., Mosaffa, A. H., & Garousi Farshi, L. (2018). Thermoeconomic assessment of a novel integrated biomass based power generation system including gas turbine cycle, solid oxide fuel cell and Rankine cycle. *Energy Conversion and Management*, *161*(November 2017), 1–12.

Gholamian, E., Zare, V., & Mousavi, S. M. (2016). Integration of biomass gasification with a solid oxide fuel cell in a combined cooling, heating and power system: A thermodynamic and environmental analysis. *International Journal of Hydrogen Energy*, *41*(44), 20396–20406.

Gu, H., Tang, Y., Yao, J., & Chen, F. (2019). Study on biomass gasification under various operating conditions. *Journal of the Energy Institute*, *92*(5), 1329–1336.

Han, J., Liang, Y., Hu, J., Qin, L., Street, J., Lu, Y., & Yu, F. (2017). Modeling downdraft biomass gasification process by restricting chemical reaction equilibrium with Aspen Plus. *Energy Conversion and Management*, *153*, 641–648.

Hosseinpour, J., Chitsaz, A., Eisavi, B., & Yari, M. (2018). Investigation on performance of an integrated SOFC-Goswami system using wood gasification. *Energy*, *148*, 614–628.

Jia, J., Shu, L., Zang, G., Xu, L., Abudula, A., & Ge, K. (2018). Energy analysis and techno-economic assessment of a co-gasification of woody biomass and animal manure, solid oxide fuel cells and micro gas turbine hybrid system. *Energy*, *149*, 750–761.

Kalina, J. (2019). Options for using solid oxide fuel cell technology in complex

integrated biomass gasification cogeneration plants. *Biomass and Bioenergy*, *122*(February), 400–413.

Karimi, M. H., Chitgar, N., Emadi, M. A., Ahmadi, P., & Rosen, M. A. (2020). Performance assessment and optimization of a biomass-based solid oxide fuel cell and micro gas turbine system integrated with an organic Rankine cycle. *International Journal of Hydrogen Energy*, *45*(11), 6262–6277.

Kumari, G., & Karmee, S. K. (2022). Thermochemical routes applying biomass: a critical assessment. In *Handbook of Biofuels* (pp. 435–451). Elsevier.

Lazzaretto, A., & Tsatsaronis, G. (2006). SPECO: A systematic and general methodology for calculating efficiencies and costs in thermal systems. *Energy*, *31*(8–9), 1257–1289.

Liu, L., Huang, Y., & Liu, C. (2016). Prediction of Rice Husk Gasification on Fluidized Bed Gasifier Based on Aspen Plus. *BioResources*, *11*(1).

Lozano, M. A., & Valero, A. (1993). Theory of the exergetic cost. *Energy*, *18*(9), 939–960.

Lv, X., Ding, X., & Weng, Y. (2019). Performance Analysis of an Intermediate-Temperature-SOFC/Gas Turbine Hybrid System Using Gasified Biomass Fuel in Different Operating Modes. *Journal of Engineering for Gas Turbines and Power*, *141*(1), 1–5

Ma, W., Xue, X., & Liu, G. (2018). Techno-economic evaluation for hybrid renewable energy system: Application and merits. *Energy*, *159*, 385–409.

McKendry, P. (2002). Energy production from biomass (part 2): conversion technologies. *Bioresource Technology*, *83*(1), 47–54.

Mekhilef, S., Saidur, R., & Safari, A. (2012). Comparative study of different fuel cell technologies. *Renewable and Sustainable Energy Reviews*, *16*(1), 981–989.

MEYER, L., TSATSARONIS, G., BUCHGEISTER, J., & SCHEBEK, L. (2009). Exergoenvironmental analysis for evaluation of the environmental impact of energy conversion systems. *Energy*, *34*(1), 75–89.

Morandin, M., Maréchal, F., & Giacomini, S. (2013). Synthesis and thermo-economic design optimization of wood-gasifier-SOFC systems for small scale applications. *Biomass and Bioenergy*, *49*, 299–314.

Ni, M. (2010). 2D thermal-fluid modeling and parametric analysis of a planar solid oxide fuel cell. *Energy Conversion and Management*, *51*(4), 714–721.

Nikoo, M. B., & Mahinpey, N. (2008). Simulation of biomass gasification in fluidized bed reactor using ASPEN PLUS. *Biomass and Bioenergy*, *32*(12), 1245–1254.

Ormerod, R. M. (2003). Solid oxide fuel cells. *Chemical Society Reviews*, *32*(1), 17–28.

Owebor, K., Oko, C. O. C., Diemuodeke, E. O., & Ogorure, O. J. (2019). Thermo-environmental and economic analysis of an integrated municipal waste-to-energy solid oxide fuel cell, gas-, steam-, organic fluid- and absorption refrigeration cycle thermal power plants. *Applied Energy*, *239*, 1385–1401.

Ozcan, H., & Dincer, I. (2015). Performance evaluation of an SOFC based trigeneration system using various gaseous fuels from biomass gasification. *International Journal of Hydrogen Energy*, *40*(24), 7798–7807.

Ozgoli, H. A., Ghadamian, H., & Pazouki, M. (2017). Economic analysis of biomass gasification-solid oxide fuel cell-gas turbine hybrid cycle. *International Journal*

of Renewable Energy Research, *7*(3), 1007–1018.

Palomba, V., Prestipino, M., & Galvagno, A. (2017). Tri-generation for industrial applications: Development of a simulation model for a gasification-SOFC based system. *International Journal of Hydrogen Energy*, *42*(46), 27866–27883.

Peksen, M., Al-Masri, A., Blum, L., & Stolten, D. (2013). 3D transient thermomechanical behaviour of a full scale SOFC short stack. *International Journal of Hydrogen Energy*, *38*(10), 4099–4107.

Peng, W., Chen, H., Liu, J., Zhao, X., & Xu, G. (2021). Techno-economic assessment of a conceptual waste-to-energy CHP system combining plasma gasification, SOFC, gas turbine and supercritical CO2 cycle. *Energy Conversion and Management*, *245*, 114622.

Perna, A., Minutillo, M., Jannelli, E., Cigolotti, V., Nam, S. W., & Yoon, K. J. (2018). Performance assessment of a hybrid SOFC/MGT cogeneration power plant fed by syngas from a biomass down-draft gasifier. *Applied Energy*, *227*(August), 80–91.

Pierobon, L., Rokni, M., Larsen, U., & Haglind, F. (2013). Thermodynamic analysis of an integrated gasification solid oxide fuel cell plant combined with an organic Rankine cycle. *Renewable Energy*, *60*, 226–234.

Puig-Arnavat, M., Bruno, J. C., & Coronas, A. (2010). Review and analysis of biomass gasification models. *Renewable and Sustainable Energy Reviews*, *14*(9), 2841–2851.

Ramzan, N., Ashraf, A., Naveed, S., & Malik, A. (2011). Simulation of hybrid biomass gasification using Aspen plus: A comparative performance analysis for food, municipal solid and poultry waste. *Biomass and Bioenergy*, *35*(9), 3962–3969.

Ranjan, K. R., & Kaushik, S. C. (2013). Energy, exergy and thermo-economic analysis of solar distillation systems: A review. *Renewable and Sustainable Energy Reviews*, *27*, 709–723.

Revankar, S. T., & Majumdar, P. (2016). *Fuel Cells*. CRC Press.

Rokni, M. (2014a). Biomass gasification integrated with a solid oxide fuel cell and Stirling engine. *Energy*, *77*, 6–18.

Rokni, M. (2014b). Thermodynamic and thermoeconomic analysis of a system with biomass gasification, solid oxide fuel cell (SOFC) and Stirling engine. *Energy*, *76*, 19–31.

Roy, D., Samanta, S., & Ghosh, S. (2019). Techno-economic and environmental analyses of a biomass based system employing solid oxide fuel cell, externally fired gas turbine and organic Rankine cycle. *Journal of Cleaner Production*, *225*, 36–57.

Safarian, S., Unnþórsson, R., & Richter, C. (2019). A review of biomass gasification modelling. *Renewable and Sustainable Energy Reviews*, *110*(May), 378–391.

Sansaniwal, S. K., Rosen, M. A., & Tyagi, S. K. (2017). Global challenges in the sustainable development of biomass gasification: An overview. *Renewable and Sustainable Energy Reviews*, *80*, 23–43.

Sezer, H., Mason, J. H., Celik, I. B., & Yang, T. (2021). Three-dimensional modeling of performance degradation of planar SOFC with phosphine exposure. *International Journal of Hydrogen Energy*, *46*(9), 6803–6816.

Shabbar, S., & Janajreh, I. (2013). Thermodynamic equilibrium analysis of coal gasification using Gibbs energy minimization method. *Energy Conversion and*

Management, *65*, 755–763.

Sharaf, O. Z., & Orhan, M. F. (2014). An overview of fuel cell technology: Fundamentals and applications. *Renewable and Sustainable Energy Reviews*, *32*, 810–853.

Shayan, E., Zare, V., & Mirzaee, I. (2019). On the use of different gasification agents in a biomass fueled SOFC by integrated gasifier: A comparative exergo-economic evaluation and optimization. *Energy*, *171*, 1126–1138.

Siefert, N. S., & Litster, S. (2014). Exergy & economic analysis of biogas fueled solid oxide fuel cell systems. *Journal of Power Sources*, *272*, 386–397.

Tavares, R., Monteiro, E., Tabet, F., & Rouboa, A. (2020). Numerical investigation of optimum operating conditions for syngas and hydrogen production from biomass gasification using Aspen Plus. *Renewable Energy*, *146*, 1309–1314.

Technology, A. (2001). *No Title*. http://web.ist.utl.pt/~ist11061/de/ASPEN/Physical_Property_Methods_and_Models.pdf

Tezer, Ö., Karabağ, N., Öngen, A., Çolpan, C. Ö., & Ayol, A. (2022). Biomass gasification for sustainable energy production: A review. *International Journal of Hydrogen Energy*, *47*(34), 15419–15433.

Toonssen, R., Sollai, S., Aravind, P. V., Woudstra, N., & Verkooijen, A. H. M. (2011). Alternative system designs of biomass gasification SOFC/GT hybrid systems. *International Journal of Hydrogen Energy*, *36*(16), 10414–10425.

Torres, C., & Valero, A. (2021). The Exergy Cost Theory Revisited. *Energies*, *14*(6), 1594.

Ud Din, Z., & Zainal, Z. A. (2016). Biomass integrated gasification–SOFC systems: Technology overview. *Renewable and Sustainable Energy Reviews*, *53*, 1356–1376.

von Spakovsky, M. R., & Evans, R. B. (1993). Engineering Functional Analysis—Part I. *Journal of Energy Resources Technology*, *115*(2), 86–92.

Wilson, L., Yang, W., Blasiak, W., John, G. R., & Mhilu, C. F. (2011). Thermal characterization of tropical biomass feedstocks. *Energy Conversion and Management*, *52*(1), 191–198.

Wongchanapai, S., Iwai, H., Saito, M., & Yoshida, H. (2012). Performance evaluation of an integrated small-scale SOFC-biomass gasification power generation system. *Journal of Power Sources*, *216*, 314–322.

Yan, L., Cao, Y., & He, B. (2019). Energy, exergy and economic analyses of a novel biomass fueled power plant with carbon capture and sequestration. *Science of the Total Environment*, *690*, 812–820.